GEOPHYSICS, VOL. 67, NO. 4 (JULY-AUGUST 2002); P. 1304–1325, 10 FIGS., 1 TABLE.
10.1190/1.1500393

In honor of the new millennium (Y2K), the SEG Research Committee is inviting a series of review articles and tutorials that summarize the state-of-the-art in various areas of exploration geophysics. Further invited contributions will appear during the next year or two—Sven Treitel, Chairman, SEG Research Subcommittee on Y2K Tutorials and Review Articles.

Y2K Review Article

Seismic modeling

José M. Carcione*, Gérard C. Herman‡, and A. P. E. ten Kroode**

ABSTRACT

Seismic modeling is one of the cornerstones of geophysical data processing. We give an overview of the most common modeling methods in use today: direct methods, integral-equation methods, and asymptotic methods. We also discuss numerical implementation aspects and present a few representative modeling examples for the different methods.

INTRODUCTION

Seismic numerical modeling is a technique for simulating wave propagation in the earth. The objective is to predict the seismogram that a set of sensors would record, given an assumed structure of the subsurface. This technique is a valuable tool for seismic interpretation and an essential part of seismic inversion algorithms. Another important application of seismic modeling is the evaluation and design of seismic surveys. There are many approaches to seismic modeling. We classify them into three main categories: direct methods, integral-equation methods, and ray-tracing methods.

To solve the wave equation by *direct methods*, the geological model is approximated by a numerical mesh, that is, the model is discretized in a finite numbers of points. These techniques are also called grid methods and full-wave equation methods, the latter since the solution implicitly gives the full wavefield. Direct methods do not have restrictions on the material variablity and can be very accurate when a sufficiently fine grid is used. Furthermore, the technique can handle the implementation of different rheologies and is well suited for the generation of snapshots which can be an important aid in the interpretation of the results. A disadvantage of these general methods, however, is that they can be more expensive than analytical and ray methods in terms of computer time.

Integral-equation methods are based on integral representations of the wavefield in terms of waves, originating from point sources. These methods are based on Huygens' principle, formulated by Huygens in 1690 in a rather heuristic way (see Figure 1). When examining Huygens' work closer, we can see that he states that the wavefield can, in some cases, be considered as a superposition of wavefields due to *volume* point sources and, in other cases, as a superposition of waves due to point sources located on a *boundary*. Both forms of Huygens' principle are still in use today and we have both volume integral equations and boundary integral equations, each with their own applications. We briefly review both methods. These methods are somewhat more restrictive in their application than the above direct methods. However, for specific geometries, such as bounded objects in a homogeneous embedding, boreholes, or geometries containing many small-scale cracks or inclusions, integral-equation methods have shown to be very efficient and to give accurate solutions. Due to their somewhat more analytic character, they have also been useful in the derivation of imaging methods based on the Born approximation. [For example, see Cohen et al. (1986) and Bleistein et al. (2001) for a description of Born inversion methods.]

Asymptotic methods or *ray-tracing methods* are very frequently used in seismic modeling and imaging. These methods are approximative, since they do not take the complete wavefield into account. On the other hand, they are perhaps the most efficient of the methods discussed in this review. Especially for large, three-dimensional models the speedup in computer time can be significant. In these methods, the wavefield is considered as an ensemble of certain events, each arriving at a certain time (traveltime) and having a certain amplitude. We discuss some of these methods, as well as some of their properties. Asymptotic methods, due to their efficiency, have played a very important role in seismic imaging based on the Born approximation for heterogeneous reference velocity models. Another important application of these methods is the modeling and identification of specific events on seismic records.

Manuscript received by the Editor January 16, 2001; revised manuscript received January 22, 2002.
*OGS, Borgo Grotta Gigante 42c, 34010 Sgonico, Trieste, Italy. E-mail: jcarcione@ogs.trieste.it.
‡Delft University of Technology, Department of Applied Analysis, Mekelweg 4, 2628 CD Delft, The Netherlands. E-mail: g.c.herman@math.tudelft.nl.
**Shell Research SIEP, Post Office Box 60, 2280 AB Rijswijk, The Netherlands.

In this overview, we discuss the above methods in some detail and give the appropriate references. In order not to get lost in tedious notations, we discuss only the acoustic formulation so we can concentrate on the differences between methods. All methods discussed here have been generalized to the elastic case and, where appropriate, references are given. We also present a few examples illustrating the applicability of the different methods. Since the applicability regions of the methods are rather different and, largely, nonoverlapping, the models are different but typical for each technique. Hopefully, they will provide the reader with some idea of the types of problems or geometries to which a particular modeling method is best suited. The modeling methods discussed here have in common that they are applicable to various two- and three-dimensional geometries. This implies that we do not discuss methods especially suited for plane-layered media, despite the fact that these methods are certainly at least as important and often used as the ones we discuss here. For an excellent overview of these plane-wave summation (or slowness) methods, see Ursin (1983).

DIRECT METHODS

We consider *finite-difference* (FD), *pseudospectral* (PS), and *finite-element* (FE) methods. These methods require the discretization of the space and time variables. Let us denote them by $(x, t) = (j\,dx, n\,dt)$, where dx and dt are the grid spacing and time step, respectively. We first introduce the appropriate mathematical formulations of the equation of motion, and then consider the main aspects of the modeling as follows: (1) time integration, (2) calculation of spatial derivatives, (3) source implementation, (4) boundary conditions, and (5) absorbing boundaries. All these aspects are discussed by using the acoustic- and SH-wave equations.

Mathematical formulations

For simplicity, we consider the acoustic- and SH-wave equations which describe propagation of compressional and pure shear waves, respectively.

Mais il faut conſiderer encore plus particulierement l'origine de ces ondes, & la maniere dont elles s'eſtendent. Et premierement il s'enſuit de ce qui à eſté dit dela production de la lumiere, que chaque petit endroit d'un corps lumineux, comme le Soleil, une chandelle, ou un charbon ardent, engendre ſes ondes, dont cet endroit eſt le centre. Ainſi dans la flame d'une chandelle, eſtans diſtinguez les points A, B, C; les cercles concentriques, decrits autour de chacun de ces points, repreſentent les ondes qui en provienent. Et il en faut concevoir de meſme autour de chaque point de la ſurface, & d'une partie du dedans de cette flame.

FIG. 1. Illustration by Huygens of Huygens' principle, stating, in French, that "each element of a light source, like the Sun, a candle or a glowing charcoal, causes waves, with the element as centre" [taken from the 1690 *Traité de la lumière* (Huygens, 1990)].

Pressure formulation

The pressure formulation for heterogeneous media can be written as (Aki and Richards, 1980, 775)

$$-L^2 p + f = \frac{\partial^2 p}{\partial t^2}, \qquad -L^2 = \rho c^2 \nabla \cdot \left(\frac{1}{\rho}\nabla\right), \tag{1}$$

where ∇ is the gradient operator, p is the pressure, c is the compressional-wave velocity, ρ is the density, and f is the body force. This is a second-order partial differential equation in the time variable.

Velocity-stress formulation

Instead of using the wave equation, wave propagation can also be formulated in terms of a system of first-order differential equations in the time and space variables. Consider, for instance, propagation of SH-waves. This is a two-dimensional phenomenon, with the particle velocity, say v_2, perpendicular to the plane of propagation. Newton's second law and Hooke's law yield the velocity-stress formulation of the SH-wave equation (Aki and Richards, 1980, 780):

$$\frac{\partial \mathbf{v}}{\partial t} = \mathbf{H}\mathbf{v} + \mathbf{F}, \tag{2}$$

where

$$\mathbf{v} = [v_2, \sigma_{32}, \sigma_{12}]^\top, \quad \mathbf{F} = [f, 0, 0]^\top, \tag{3}$$

$$\mathbf{H}\mathbf{v} = \mathbf{A}\frac{\partial \mathbf{v}}{\partial x_1} + \mathbf{B}\frac{\partial \mathbf{v}}{\partial x_3}, \tag{4}$$

$$\mathbf{A} = \begin{pmatrix} 0 & 0 & \rho^{-1} \\ 0 & 0 & 0 \\ \mu & 0 & 0 \end{pmatrix}, \quad \mathbf{B} = \begin{pmatrix} 0 & \rho^{-1} & 0 \\ \mu & 0 & 0 \\ 0 & 0 & 0 \end{pmatrix}, \tag{5}$$

and σ denotes stress and μ is the shear modulus.

The solution to equation (2) subject to the initial condition $\mathbf{v}(0) = \mathbf{v}_0$ is formally given by

$$\mathbf{v}(t) = \exp(t\mathbf{H})\mathbf{v}_0 + \int_0^t \exp(\tau\mathbf{H})\,\mathbf{F}(t-\tau)\,d\tau, \tag{6}$$

where $\exp(t\mathbf{H})$ is called the evolution operator, because application of this operator to the initial condition vector (or to the source vector) yields the solution at time t. We refer to $\mathbf{H}$ as the propagation matrix. The SH and acoustic differential equations are hyperbolic (Jain, 1984, 251; Smith, 1985, 4) because the field has a finite velocity.

Variational formulation

The most standard finite-element method uses the wave equation (1) as a starting point. We consider a volume V bounded by a surface S. The surface S is divided into S_p, where pressure boundary conditions are defined, and S_{dp}, the part on which normal accelerations (or pressure fluxes) are given. Assume a small pressure variation δp which is consistent with the boundary conditions. If we multiply equation (1) by δp, integrate over the volume V and by parts (using the divergence theorem), we obtain

$$\int_V \frac{1}{\rho}\nabla\delta p \cdot \nabla p\,dV = -\int_V \frac{\delta p}{\rho c^2}\frac{\partial^2 p}{\partial t^2}\,dV + \int_V \frac{f\,\delta p}{\rho c^2}\,dV + \int_{S_{dp}} \frac{\delta p}{\rho}\mathbf{n}\cdot\nabla p\,dS, \tag{7}$$

where **n** is the normal to the surface S. This variational formulation derived from the wave equation is equivalent to a Galerkin procedure (Zienkiewicz, 1977, 70; Hughes, 1987, 7).

Time integration

The numerical solution of the wave equation requires the discretization of the time variable by using finite differences (an exception to this is formed by the spectral methods; see below). The basic idea underlying FD methods is to replace the partial derivatives by approximations based on Taylor series expansions of functions near the point of interest. Forward and backward difference approximations of the time derivatives (Smith, 1985, 7) lead to explicit and implicit FD schemes, respectively. Explicit means that the wavefield at present time is computed from the wavefield at past times. On the other hand, in implicit methods, the present values depend on past and future values. Unlike explicit methods, implicit methods are unconditionally stable but lead to a great amount of computation arising from the need to carry out large matrix inversions. In general, the differential formulation of the wave equation is solved with explicit algorithms, since the time step is determined by accuracy criteria rather than by stability criteria (Emerman et al., 1982).

Eigenvalues and stability

Wave equations used in seismic exploration and seismology can be expressed as $\dot{\mathbf{v}} = \mathbf{H}\mathbf{v}$, where **H** is the propagation matrix containing the material properties and spatial derivatives (the dot denotes time differentiation) [e.g., equation (2)]. We now address the stability aspects of finite-difference schemes and therefore consider the eigenvalue problem of wave propagation. Assume constant material properties and a plane-wave kernel of the form $\exp(i\mathbf{k}\cdot\mathbf{x} - i\omega t)$, where **k** is the wavenumber vector, **x** is the position vector, and ω is the angular frequency (which can be complex valued in the case of attenuation). Substitution of the plane-wave kernel into the wave equation yields an eigenvalue equation for the eigenvalues $\lambda = -i\omega$. For the acoustic- and SH-wave equations, these eigenvalues lie on the imaginary axis of the λ-plane. For instance, in 1-D space, the eigenvalues corresponding to equations (1) and (2) are $\lambda = \pm ikc$, where c is either the compressional- or the shear-wave velocity. There are other equations of interest in seismic modeling in which eigenvalues might lie in the left-hand λ-plane. Some of these are discussed below.

Consider an anelastic medium described by a viscoelastic stress-strain relation. Wave attenuation is governed by material relaxation times, which quantify the response time of the medium to a perturbation (lossless solid materials respond instantaneously, i.e., the relaxation time is zero). For a viscoelastic medium with moderate attenuation, the eigenvalues have a small negative real part causing the waves to be attenuated. In addition, when solving the equations in the time domain, there are eigenvalues with a large negative part and close to the real axis that are approximately given by the reciprocal of the relaxation times corresponding to each attenuation mechanism. Then, the domain of the eigenvalues has a T shape (see Tal-Ezer et al., 1990). If the central frequency of these relaxation peaks is close to the source frequency band, or equivalently, if the related eigenvalues are close to the imaginary axis of the λ-plane, an explicit scheme performs very efficiently.

The situation is critical for porous media, where the eigenvalue corresponding to the slow compressional wave at seismic frequencies (a quasi-static mode) has a very large negative part, which is related to the location of Biot relaxation peaks, usually beyond the sonic band for pore fluids like water and oil (Carcione and Quiroga-Goode, 1996). When the modulus of the eigenvalues is very large compared to the inverse of the maximum propagation time, the differential equation is said to be stiff (Jain, 1984, 72; Smith, 1985, 198). Due to the presence of the quasi-static slow wave, the low-frequency Biot differential equations are hyperbolic/parabolic. Although the best algorithm would be an implicit method, the problem can still be solved with explicit methods (see below).

Time and space discretization of the wave equation with an explicit scheme (forward time difference only) leads to an equation of the form $\mathbf{v}^{n+1} = \mathbf{G}\mathbf{v}^n$, where **G** is called the amplification matrix. The von Neumann condition for stability requires $\max|g_j| \le 1$, where g_j are the eigenvalues of **G** (Jain, 1984, 418). It can be shown that this condition does not hold for all dt when explicit schemes are used, and that implicit schemes do not have any restriction. For instance, explicit fourth-order Taylor and Runge-Kutta methods require $dt|\lambda\ \max| < 2.78$ (Jain, 1984, 71), implying very small time steps for very large eigenvalues. Implicit methods are A-stable (Jain, 1984, 118), meaning that the domain of convergence is the left open-half λ-plane.

Classical finite differences

Evaluating the second time derivative in equation (1) at $(n+1)\,dt$ and $(n-1)\,dt$ by a Taylor expansion, and summing both expressions, yields

$$\frac{\partial^2 p^n}{\partial t^2} = \frac{1}{dt^2}\left[p^{n+1} + p^{n-1} - 2p^n - 2\sum_{\ell=2}^{\mathrm{L}} \frac{dt^{2\ell}}{(2\ell)!}\frac{\partial^{2\ell} p^n}{\partial t^{2\ell}}\right]. \tag{8}$$

The wave equation (1) provides the higher order time derivatives, using the following recursion relation:

$$\frac{\partial^{2\ell} p^n}{\partial t^{2\ell}} = -L^2\frac{\partial^{2\ell-2} p^n}{\partial t^{2\ell-2}} + \frac{\partial^{2\ell-2} f^n}{\partial t^{2\ell-2}}. \tag{9}$$

This algorithm, where high-order time derivatives are replaced by spatial derivatives, is often referred to as the Lax-Wendroff scheme (Jain, 1984, 415; Smith, 1985, 181; Dablain, 1986; Blanch and Robertsson, 1997). A Taylor expansion of the evolution operator $\exp(dt\mathbf{H})$ is equivalent to a Lax-Wendroff-scheme.

The dispersion relation connects the frequency with the wavenumber and allows the calculation of the phase velocity corresponding to each Fourier component. Time discretization implies an approximation of the dispersion relation, which in the continuous case is $\omega = ck$, with ω the angular frequency. Assuming constant material properties and a 1-D wave solution of the form $\exp(ikx - i\bar{\omega}n\,dt)$, where k is the wavenumber and $\bar{\omega}$ is the FD angular frequency, yields the following dispersion relation:

$$\frac{2}{dt}\sin\left(\frac{\bar{\omega}\,dt}{2}\right) = ck\sqrt{1 - 2\sum_{\ell=2}^{\mathrm{L}}(-1)^{\ell}\frac{(ck\,dt)^{2\ell-2}}{(2\ell)!}}. \tag{10}$$

The FD approximation to the phase velocity is $\bar{c} = \bar{\omega}/k$. Using equation (10) with second-order accuracy [neglect $O(dt^2)$ terms], the FD phase velocity is

$$\bar{c} = \frac{c}{|\mathrm{sinc}(\theta)|}, \quad \theta = \bar{f}\, dt, \tag{11}$$

where $\bar{\omega} = 2\pi\, \bar{f}$ and $\mathrm{sinc}(\theta) = \sin(\pi\theta)/(\pi\theta)$. Equation (11) indicates that the FD velocity is greater than the true phase velocity. Since $\bar{\omega}$ should be a real quantity, thus avoiding exponentially growing solutions, the value of the sine function in equation (10) must be between -1 and 1. This constitutes the stability criterion. For instance, for second-order time integration this means $ck\, dt/2 \le 1$. The maximum phase velocity, $c_{\max}$, and the maximum wavenumber (i.e. the Nyquist wavenumber, $\pi/dx_{\min}$) must be considered. Then, the condition is

$$dt \le s\left(\frac{dx_{\min}}{c_{\max}}\right), \quad s = \frac{2}{\pi}. \tag{12}$$

A rigorous demonstration, based on the amplification factor, is given by Smith (1985, 70; see also Celia and Gray, 1992, 232). In n-D space, $s = 2/(\pi\sqrt{n})$ and, for a fourth-order approximation (L = 2) in 1-D space, $s = 2\sqrt{3}/\pi$. Equation (12) indicates that stability is governed by the minimum grid spacing and the higher velocities.

Let us now consider the presence of attenuation. Time-domain modeling in lossy media can be described by viscoelastic stress-strain relations. This requires the use of the so-called memory variables, one for each relaxation mechanism (Carcione et al., 1988). The introduction of additional differential equations for these field variables avoids the numerical computation of the viscoelastic convolution integrals. The differential equation for a memory variable e has the form

$$\frac{\partial e}{\partial t} = a\epsilon - be, \quad b > 0, \tag{13}$$

where ϵ is a field variable (e.g., the dilatation) and a and b are material properties (b is approximately the central frequency of the relaxation peak). Equation (13) can be discretized by using the central differences operator for the time derivative $[dt(\partial e/\partial t)^n = e^{n+1} - e^{n-1}]$ and mean value operator for the memory variable $(2e^n = e^{n+1} + e^{n-1})$. These approximations are used in the Crank-Nicolson scheme (Smith, 1985, 19). This approach leads to an explicit algorithm

$$e^{n+1/2} = \frac{2\, dt\, a}{2 + b\, dt}\epsilon^n + \left(\frac{2 - b\, dt}{2 + b\, dt}\right)e^{n-1/2} \tag{14}$$

(Emmerich and Korn, 1987). This method is robust in terms of stability, because the coefficient of $e^{n-1/2}$, related to the viscoelastic eigenvalue of the amplification matrix, is less than 1 for any value of the time step dt. The same method performs equally well for wave propagation in porous media (Carcione and Quiroga-Goode, 1996).

Splitting methods

Time integration can also be performed with the method of dimensional splitting, also called Strang's scheme (Jain, 1984, 444; Mufti, 1985; Bayliss et al., 1986; Vafidis et al., 1992). Consider equation (2) and denote a derivative with respect to a variable ϕ by the subscript "$,\phi$". The 1-D equations $\mathbf{v}_{,t} = \mathbf{A}\mathbf{v}_{,x_1}$ and $\mathbf{v}_{,t} = \mathbf{B}\mathbf{v}_{,x_3}$ are solved by means of one-dimensional difference operators $\mathbf{L}_{x_1}$ and $\mathbf{L}_{x_3}$, respectively. For instance, Bayliss et al. (1986) use a fourth-order accurate predictor-corrector scheme and the splitting algorithm $\mathbf{v}^{n+2} = \mathbf{L}_{x_1}\mathbf{L}_{x_3}\mathbf{L}_{x_3}\mathbf{L}_{x_1}\mathbf{v}^n$, where each operator advances the solution by a half time step. The maximum allowed time step is larger than for unsplit schemes, because the stability properties are determined by the 1-D schemes. Splitting is also useful when the system of differential equations is stiff. For instance, Biot's poroelastic equations can be partitioned into a stiff part and a nonstiff part, so that the evolution operator can be expressed as $\exp(\mathbf{H}_r + \mathbf{H}_s)t$, where r indicates the regular matrix and s the stiff matrix. The product formulas $\exp(\mathbf{H}_r t)\exp(\mathbf{H}_s t)$ and $\exp(\frac{1}{2}\mathbf{H}_s t)\exp(\mathbf{H}_r t)\exp(\frac{1}{2}\mathbf{H}_s t)$ are first- and second-order accurate, respectively. The stiff part can be solved analytically and the nonstiff part with an standard explicit method (Carcione and Quiroga-Goode, 1996). Strang's scheme can be shown to be equivalent to the splitting of the evolution operator for solving the poroelastic equations.

Predictor-corrector schemes

Predictor-corrector schemes of different order find wide application in seismic modeling (Mufti, 1985; Bayliss et al., 1986; Vafidis et al., 1992; Dai et al., 1995). Consider equation (2) and the first-order approximation

$$\bar{\mathbf{v}}^{n+1} = \mathbf{v}^n + dt\, \mathbf{H}\mathbf{v}^n, \tag{15}$$

known as the forward Euler scheme. This solution is given by the intersection point between the tangent of $\mathbf{v}$ at $t = n\, dt$ and the line $t = (n+1)\, dt$. A second-order approximation can be obtained by averaging this tangent with the predicted one. Then, the corrector is

$$\mathbf{v}^{n+1} = \mathbf{v}^n + \frac{dt}{2}(\mathbf{H}\mathbf{v}^n + \mathbf{H}\bar{\mathbf{v}}^{n+1}). \tag{16}$$

This algorithm is the most simple predictor-corrector scheme (Celia and Gray, 1992, 64). A predictor-corrector MacCormack scheme, second-order in time and fourth-order in space, is used by Vafidis et al. (1992) to solve the elastodynamic equations.

Spectral methods

As mentioned before, a Taylor expansion of the evolution operator $\exp(dt\mathbf{H})$ is equivalent to a Lax-Wendroff-scheme. When the number of terms in equation (8) is increased, a larger time step can be used while retaining high accuracy. Taylor expansions and Runge-Kutta methods, however, are not the best in terms of accuracy. The evolution operator in equation (6) can be expanded in terms of Chebyshev polynomials as

$$\mathbf{v}(t) = \sum_{k=0}^{M} C_k\, J_k(tR)\, Q_k\left(\frac{\mathbf{H}}{R}\right)\mathbf{v}_0, \tag{17}$$

where $C_0 = 1$ and $C_k = 2$ for $k \neq 0$, J_k is the Bessel function of order k, and Q_k are modified Chebyshev polynomials. R should be chosen larger than the absolute value of the eigenvalues of $\mathbf{H}$ (Tal-Ezer et al., 1987). This technique allows the calculation of the wavefield with large time steps. Chebyshev expansions are optimal since they require the minimum number of terms. The most time-consuming part of a modeling algorithm is the evaluation of the terms $-L^2 p$ in equation (1) or $\mathbf{H}\mathbf{v}$ in equation (2) due to the computation of the spatial derivatives.

A Taylor-expansion algorithm needs $N = t_{\max}/dt$ of such evaluations to compute the solution at time $t_{\max}$. On the other hand, the number of evaluations using equation (17) is equal to the number of terms in the Chebyshev expansion. Numerical tests indicate that M is comparable to N for second-order finite differencing, but the error of the Chebyshev operator is practically negligible for single-precision programming (Tal-Ezer et al., 1987). This means that there is no numerical dispersion due to the time integration.

When the wave equation is used, which is second order in time [see equation (1)], the rapid-expansion method (REM method) is twice as efficient since the expansion then contains only even-order Chebyshev functions (Kosloff et al., 1989). A similar algorithm for the viscoelastic wave equation is developed by Tal-Ezer et al. (1990). These methods are said to have spectral accuracy, in the sense that the error of the approximation tends exponentially to zero when the degree of the approximating polynomial increases.

Algorithms for finite-element methods

In the FE method, which can be derived from the variational formulation (7), the field variables are evaluated by interpolation from nodal (grid) values. For a second-order isoparametric method (Zienkiewicz, 1977, 178; Hughes, 1987, 118), the interpolation can be written as

$$p(x_i) = \mathbf{\Phi}^\top \mathbf{P}, \tag{18}$$

where $\mathbf{P}$ is a column vector of the values $p(x_i)$ at the nodes, and $\mathbf{\Phi}^\top$ is a row vector of spatial interpolation functions, also referred to as shape and basis functions. The approximation to equation (7) is obtained by considering variations δp according to the interpolation (18). Since $\delta p = \mathbf{\Phi}^\top \delta \mathbf{P}$, and $\delta \mathbf{P}$ is arbitrary, the result is a set of ordinary differential equations at the nodal pressures $\mathbf{P}$ (Zienkiewicz, 1977, 531; Hughes, 1987, 506):

$$\mathbf{K}\mathbf{P} + \mathbf{M}\frac{\partial^2 \mathbf{P}}{\partial t^2} + \mathbf{S} = 0, \tag{19}$$

where $\mathbf{K}$ is the stiffness matrix, $\mathbf{M}$ is the mass matrix, and $\mathbf{S}$ is the generalized source matrix. These matrices contain volume integrals that are evaluated numerically (see also the "The finite-element method" section). The matrix $\mathbf{M}$ is often replaced by a diagonal lumped mass matrix $\hat{\mathbf{M}}$ such that each entry equals the sum of all entries in the same row of $\mathbf{M}$ (Zienkiewicz, 1977, 535). In this way, the solution can be obtained with an explicit time-integration method, such as the central difference method (Serón et al., 1990). This technique can be used with low-order interpolation functions, for which the error introduced by the algorithm is relatively low. When high-order polynomials (including Chebyshev polynomials) are used as interpolation functions, the system of equations (19) is generally solved with implicit algorithms. In this case, the most popular algorithm is the Newmark method (Hughes, 1987, 490; Padovani et al., 1994; Serón et al., 1996).

Finally, numerical modeling can be performed in the frequency domain. The method is very accurate but generally expensive when using differential formulations, because it involves the solution of many Helmholtz equations (Jo et al., 1996). It is used more in FE algorithms (Marfurt, 1984; Santos et al., 1988; Kelly and Marfurt, 1990).

Calculation of spatial derivatives

The name of a particular modeling method is usually derived from the algorithm for computing the spatial derivatives. The following sections briefly review these algorithms.

Finite differences

FD methods use either homogeneous or heterogeneous formulations to solve the equation of motion. In the first case, the motion in each homogeneous region is described by the equation of motion with constant acoustic parameters. For this method, boundary conditions across all interfaces must be satisfied explicitly. The heterogeneous formulation incorporates the boundary conditions implicitly by constructing FD representations using the equation of motion for heterogeneous media. The homogeneous formulation is of limited use because it can only be used efficiently for simple, piecewise homogeneous geometries. The heterogeneous formulation, on the other hand, makes it possible to assign different acoustic properties to every grid point, providing the flexibility to simulate a variety of complex subsurface models (e.g., random media or velocity gradients). Heterogeneous formulations generally make use of staggered grids to obtain stable schemes for large variations of Poisson's ratio (Virieux, 1986). In staggered grids, groups of field variables and material properties are defined on different meshes separated by half the grid spacing (Fornberg, 1996, 91). The newly computed variables are centered between the old variables. Staggering effectively halves the grid spacing, increasing the accuracy of the approximation.

Seismic modeling in heterogeneous media requires the calculation of first derivatives. Consider the following approximation with an even number of points, suitable for staggered grids:

$$\frac{\partial p_0}{\partial x} = w_0(p_{\frac{1}{2}} - p_{-\frac{1}{2}}) + \cdots + w_\ell(p_{\ell+\frac{1}{2}} - p_{-\ell-\frac{1}{2}}), \tag{20}$$

with ℓ weighting coefficients w_ℓ. The antisymmetric form guarantees that the derivative is zero for even powers of x. Let us test the spatial derivative approximation for $p = x$ and $p = x^3$. Requiring that equation (20) be accurate for all polynomials up to order 2 yields the approximation $(p_{\frac{1}{2}} - p_{-\frac{1}{2}})/dx$, while for fourth accuracy [the leading error term is $O(dx^4)$] the weights are obtained from $w_0 + 3w_1 = 1/dx$ and $w_0 + 27w_1 = 0$, giving $w_0 = 9/(8\,dx)$, and $w_1 = -1/(24\,dx)$ (Fornberg, 1996, 91). To obtain the value of the derivative at $x = j\,dx$, substitute subscript 0 with j, $\ell + \frac{1}{2}$ with $j + \ell + \frac{1}{2}$ and $-\ell - \frac{1}{2}$ with $j - \ell - \frac{1}{2}$. Fornberg (1996, 15) provides an algorithm for computing the weights of first and second spatial derivatives for the general case, i.e., approximations which need not be evaluated at a gridpoint such as centered and one-sided derivatives. He also shows that the FD coefficients w_ℓ in equation (20) are equivalent to those of the Fourier PS method when ℓ approaches the number of grid points (Fornberg, 1996, 34).

Let us now study the accuracy of the approximation by considering the dispersion relation. Assuming constant material properties and a 1-D wave solution of the form $\exp(i\bar{k}\,j\,dx - i\omega t)$, the second-order approximation gives the following FD dispersion relation and phase velocity:

$$\omega^2 = c^2\bar{k}^2 \mathrm{sinc}^2(\psi), \qquad \bar{c} = c|\mathrm{sinc}(\psi)|, \tag{21}$$

where $\psi = \bar{K}\,dx$, with $\bar{k} = 2\pi\bar{K}$ [equation (21) can be derived in the same manner as equation (11)]. The spatial dispersion acts in the opposite sense of temporal dispersion [see equation (11)]. Thus, the FD velocity is smaller than the true phase velocity.

Staggered grids improve accuracy and stability, and eliminate noncausal artifacts (Virieux, 1986; Levander, 1988; Özdenvar and McMechan, 1997; Carcione and Helle, 1999). Staggered grid operators are more accurate than centered differences operators in the vicinity of the Nyquist wavenumber (e.g., Kneib and Kerner, 1993). The velocity-stress formulation in staggered grids constitutes a flexible modeling technique because it allows one to freely impose boundary conditions (see the "Boundary conditions" section) and is able to directly yield all the field variables (Karrenbach, 1998).

However, there is a disadvantage in using staggered grids for anisotropic media of symmetry lower than orthorhombic. Staggering implies that the off-diagonal stress and strain components are not defined at the same location. When evaluating the stress-strain relation, it is necessary to sum over a linear combination of the elasticity constants (c_{IJ}, $I, J = 1, \ldots 6$) multiplied by the strain components. Hence, some terms of the stress components have to be interpolated to the locations where the diagonal components are defined (Mora, 1989).

A physical criterion to improve accuracy is to compute the weights w_ℓ in equation (20) by minimizing the relative error in the components of the group velocity $c_g = \partial\omega/\partial k$ (the velocity of a wave packet). This procedure, combined with grid staggering and a convolutional scheme, yields an optimal differential operator for wave equations (Holberg, 1987). The method is problem dependent because it depends on the type of wave equation. Igel et al. (1995) obtained high accuracy with operators of small length (eight points) in the anisotropic case. The treatment of the *P-SV* case and more details about the finite difference approximation are in Levander (1989).

The modeling can be made more efficient by using hybrid techniques, for instance, combining finite differences with faster algorithms such as ray-tracing methods (Robertsson et al., 1996), integral-equation methods (Stead and Helmberger, 1988), and reflectivity methods (Emmerich, 1989). In this way, modeling of the full wavefield can be restricted to the target (e.g., the reservoir), and propagation in the rest of the model (e.g., the overburden) can be simulated with faster methods.

Pseudospectral methods

The pseudospectral methods used in forward modeling of seismic waves are mainly based on the Fourier and Chebyshev differential operators. Gazdag (1981) first and Kosloff and coworkers later applied the technique to seismic exploration problems (e.g., Kosloff and Baysal, 1982; Reshef et al., 1988). Mikhailenko (1985) combined transforms methods (e.g., Bessel transforms) with FD and analytical techniques.

The sampling points of the Fourier method are $x_j = j\,dx = j\,x_{\max}/(N_x - 1)$ $(j = 0, \ldots, N_x - 1)$, where $x_{\max}$ is the maximum distance and N_x is the number of grid points. For a given function $f(x)$, with Fourier transform $\tilde{f}(k)$, first and second derivatives are computed as

$$\widetilde{\frac{\partial f}{\partial x}} = ik\,\tilde{f}, \qquad \widetilde{\frac{\partial^2 f}{\partial x^2}} = -k^2\,\tilde{f}, \tag{22}$$

where k is the discrete wavenumber. The transform $\tilde{f}$ to the wavenumber domain and the transform back to the space domain are calculated by the fast Fourier transform (FFT). The derivatives of two real functions—two adjacent grid lines of the computational mesh—can be computed by two complex (direct and inverse) FFTs. The two functions are put into the real and imaginary parts, the FFT is performed, the result is multiplied by ik, and the inverse FFT gives the derivatives in the real and imaginary parts. Staggered operators that evaluate first derivatives between grid points are given by

$$D_x^{\pm}\phi = \sum_{k=0}^{k(N_x)} ik\exp(\pm ik\,dx/2)\tilde{\phi}(k)\exp(ikx), \tag{23}$$

where $k(N_x) = \pi/dx$ is the Nyquist wavenumber. The standard differential operator is given by the same expression, without the phase shift term $\exp(\pm ik\,dx/2)$. The standard operator requires the use of odd-based FFTs (i.e., N_x should be an odd number). This is because even transforms have a Nyquist component which does not possess the Hermitian property of the derivative (Kosloff and Kessler, 1989). When $\phi(x)$ is real, $\tilde{\phi}(k)$ is Hermitian (i.e., its real part is even and its imaginary part is odd). If N_x is odd, the discrete form of k is an odd function, therefore $ik\tilde{\phi}(k)$ is also Hermitian and the derivative is real. On the other hand, the first derivative computed with the staggered differential operator is evaluated between grid points and uses even-based Fourier transforms. The approximation (23) is accurate up to the Nyquist wavenumber. If the source spectrum is negligible beyond the Nyquist wavenumber, we can consider that there is no significant numerical dispersion due to the spatial discretization. Hence, the dispersion relation is given by equation (10), which for a second-order time integration can be written as

$$\bar{\omega} = \frac{2}{dt}\sin^{-1}\left(\frac{ck\,dt}{2}\right). \tag{24}$$

Because k should be real to avoid exponentially growing solutions, the argument of the inverse sine must be less than one. This implies the stability condition $k_{\max}c\,dt/2 \le 1$, which leads to $\alpha \equiv c\,dt/dx \le 2/\pi$, since $k_{\max} = \pi/dx$ (α is called the Courant number). Generally, a criterion $\alpha < 0.2$ is used to choose the time step (Kosloff and Baysal, 1982). The Fourier method has periodic properties. In terms of wave propagation this means that a wave impinging on the left boundary of the grid will return from the right boundary (the numerical artifact called wraparound).

The Chebyshev method is mainly used in the velocity-stress formulation to model free surface, rigid, and nonreflecting boundary conditions at the boundaries of the mesh. Chebyshev transforms are generally computed with the FFT, with a length twice of that used by the Fourier method (Gottlieb and Orszag, 1977, 117). Since the sampling points are very dense at the edges of the mesh, the Chebyshev method requires a 1-D stretching transformation to avoid very small time steps [see equation (12)]. Because the grid cells are rectangular, mapping transformations are also used for modeling curved interfaces to obtain an optimal distribution of grid points (Fornberg, 1988; Carcione, 1994a) and model surface topography (Tessmer and Kosloff, 1994).

The Fourier and Chebyshev methods are accurate up to the maximum wavenumber of the mesh that corresponds to

a spatial wavelength of two grid points (at maximum grid spacing for the Chebyshev operator). This fact makes these methods very efficient in terms of computer storage (mainly in 3-D space) and makes the Chebyshev technique highly accurate for simulating Neumann and Dirichlet boundary conditions, such as stress-free and rigid conditions (Carcione, 1994a, b) (see the "Boundary conditions" section).

The finite-element method

The FE method has two advantages over FD and PS methods, namely, its flexibility in handling boundary conditions and irregular interfaces. On the basis of equation (18), consider the 1-D case, with uniform grid spacing dx, and an element whose coordinates are X_1 and X_2 ($X_2 - X_1 = dx$) and whose nodal pressures are P_1 and P_2. This element is mapped into the interval $[-1, 1]$ in a simplified coordinate system (the reference Z-system). Denote the physical variable by x and the new variable by z. The linear interpolation functions are

$$\phi_1 = \frac{1}{2}(1 - z), \qquad \phi_2 = \frac{1}{2}(1 + z). \tag{25}$$

If the field variable and the independent (physical) variable are computed by using the same interpolation functions, one has the so-called isoparametric approach (Hughes, 1987, 20). That is,

$$p = \phi_1 P_1 + \phi_2 P_1, \qquad x = \phi_1 X_1 + \phi_2 X_1. \tag{26}$$

Assembling the contributions of all the elements of the stiffness matrix results in a centered second-order differencing operator if the density is constant. When the density is variable, the stiffness matrix is equivalent to a staggered FD operator (Kosloff and Kessler, 1989).

FE methods have been used to solve problems in seismology, in particular, propagation of Love and Rayleigh waves in the presence of surface topography (Lysmer and Drake, 1972; Schlue, 1979). FE applications for seismic exploration require, in principle, more memory and computer time than the study of surface waves (as used in modeling soil-structure interaction). In fact, the problem of propagation of seismic waves from the surface to the target (the reservoir) involves the storage of large matrices and much computer time. During the 1970s and 1980s, the effort was in rendering efficient existing low-order FE techniques rather than proposing new algorithms. Moreover, it turns out that besides the physical propagation modes, there are parasitic modes when high-order FE methods are used (Kelly and Marfurt, 1990). These parasitic modes are nonphysical solutions of the discrete dispersion relation obtained from the von Neumann stability analysis. For instance, for a 2-D cubic element grid, there are ten modes of propagation: two corresponding to the P- and SV-waves, and eight parasitic modes of propagation.

This was the state of the art at the end of the 1980s. In the 1990s. Serón et al. (1990, 1996) further developed the computational aspects of low-order FE to make them more efficient for seismic exploration problems.

High-order FE methods became more efficient with the advent of the spectral element method (SPEM) (Seriani et al., 1992; Padovani et al., 1994; Priolo et al., 1994; Komatitsch and Vilotte, 1998). In this method, the approximation functional space is based on high-order orthogonal polynomials having spectral accuracy (i.e., the rate of convergence is exponential with respect to the polynomial order). Consider, for instance, the 2-D case and the acoustic wave equation. The physical domain is decomposed into nonoverlappring quadrilateral elements. In each element, the pressure field $p(z_1, z_2)$, defined on the square interval $[-1, 1] \times [-1, 1]$ in the reference system Z, is approximated by the product

$$p(z_1, z_2) = \sum_{i=0}^{N} \sum_{j=0}^{N} P_{ij} \phi_i(z_1) \phi_j(z_2). \tag{27}$$

In this expansion, P_{ij} are the nodal pressures and ϕ_i are Lagrangian interpolants that satisfy the relation $\phi_i(\zeta_k) = \delta_{ik}$ within the interval $[-1, 1]$ and vanish outside (δ_{ik} denotes the Kronecker delta and ζ_k stands for z_1 and z_2). The Lagrangian interpolants are given by

$$\phi_j(\zeta) = \frac{2}{N} \sum_{n=0}^{N} \frac{1}{c_j c_n} T_n(\zeta_j) T_n(\zeta), \tag{28}$$

where T_n are Chebyshev polynomials, ζ_j are the Gauss-Lobatto quadrature points, and $c_0 = c_N = 0$, $c_n = 1$ for $1 \le n \le N$. The Chebyshev functions are also used for the mapping transformation between the physical world X and the local system Z. Seriani et al. (1992) used Chebyshev polynomials from eighth order to fifteenth order. This allows up to three points per minimum wavelength without generating parasitic or spurious modes, and computational efficiency is improved by about one order of magnitude compared to low-order FE. If the meshing of a geological structure is as regular as possible (i.e., with a reasonable aspect ratio for the elements), the matrices are well conditioned and an iterative method such as the conjugate gradient uses less than eight iterations to solve the implicit system of equations.

Source implementation

The basic seismic sources are a directional force, a pressure source, and a shear source, simulating, for instance, a vertical vibrator, an explosion, or a shear vibrator. Complex sources, such as earthquakes sources, can be represented by a set of directional forces [e.g., a double couple (Aki and Richards, 1980, 82)].

Consider an elastic formulation of the wave equation, that is, P- and S-wave propagation (Kosloff et al., 1984). A directional force vector has components $f_i = a(x_i) h(t) \delta_{im}$, where a is a spatial function (usually a Gaussian), $h(t)$ is the time history, δ denotes the Kronecker delta function, and m is the source direction. A pressure source can be obtained from a potential of the form $\phi = a(x_i) h(t)$ as $f_i = \partial \phi / \partial x_i$. A shear source is of the form $\mathbf{f} = \nabla \times \mathbf{A}$, where $\mathbf{A}$ is a vector potential. In 2-D space, $\mathbf{A} = (0, A)$ with $A = a(x_i) h(t)$. In velocity-stress formulations, the source can be introduced as described above or in the constitutive equations (stress-strain relations) such that a pressure source implies $\sigma_{11} = \sigma_{22} = \sigma_{33}$ initially at the source location, and shear sources result from a stress tensor with zero trace (e.g., Bayliss et al., 1986).

Introducing the source in a homogeneous region by imposing the values of the analytical solution should handle the singularity at the source point. Many FD techniques (Kelly et al., 1976;

Virieux, 1986) are based on the approach of Alterman and Karal (1968). The numerical difficulties present in the vicinity of the source point are solved by subtracting the field due to the source from the total field due to reflection, refraction, and diffractions in a region surrounding the source point. This procedure inserts the source on the boundary of a rectangular region. The direct source field is computed analytically. This method has been recently used by Robertsson and Chapman (2000) to "inject" a numerical wavefield into a FD mesh. Their approach allows for efficient computation of many common-shot experiments after alterations of the seismic model in a subarea containing the target (e.g., the reservoir).

When solving the velocity-stress formulation with pseudospectral (PS) algorithms and high-order FD methods (Bayliss et al., 1986), the source can be implemented in one grid point in view of the accuracy of the differential operators. Numerically (in 1-D space and uniform grid spacing), the strength of a discrete delta function in the spatial domain is $1/dx$, where dx is the grid size. Since each spatial sample is represented by a sinc function with argument x/dx (the spatial integration of this function is precisely dx), the introduction of the discrete delta will alias the wavenumbers beyond the Nyquist (π/dx) to the lower wavenumbers. However, if the source time-function $h(t)$ is band limited with cut-off frequency $f_{\max}$, the wavenumbers greater than $k_{\max} = 2\pi f_{\max}/c$ will be filtered. Moreover, since the wave equation is linear, seismograms with different time histories can be implemented by convolving $h(t)$ with only one simulation obtained with $\delta(t)$ as a source (a discrete delta with strength $1/dt$).

The computation of synthetic seismograms for simulating zero-offset (stacked) seismic sections requires the use of the exploding-reflector concept (Loewenthal et al., 1976) and the so-called nonreflecting wave equation (Baysal et al., 1984). A source proportional to the reflection coefficients is placed on the interfaces and is initiated at time zero. All the velocities must be halved in order to get the correct arrival times. The nonreflecting condition implies a constant impedance model to avoid multiple reflections, which are, in principle, absent from stacked sections and constitute unwanted artifacts in migration processes.

Boundary conditions

Free-surface and interface boundary conditions are the most important in seismic exploration and seismology. Although in FE methods the implementation of traction-free boundary conditions is natural (simply do not impose any constraint at the surface nodes), FD and PS methods require a special boundary treatment. However, some restrictions arise in FE and FD modeling when large values of the Poisson's ratio (or V_P/V_S ratio) occur at a free surface.

Consider first the free-surface boundary condition. The classical algorithm used in FD methods (e.g., Kelly et al., 1976) is to include a fictitious line of grid points above the surface, and use one-sided differences to approximate normal derivatives and centered differences to approximate tangential derivatives. This simple low-order scheme has an upper limit of $V_P/V_S \leq 0.35$, where V_P and V_S are the P-wave and S-wave velocities. Moreover, the method is inaccurate due to the use of one-sided differences. The use of a staggered differential operator and radiation conditions of the paraxial type (see below) is effective for large variations of Poisson's ratio (Virieux, 1986).

The traction-free condition at the surface of the earth can be obtained by including a wide zone on the upper part of the mesh containing zero values of the stiffnesses [the so-called zero-padding technique (Kosloff et al., 1984)]. Whereas for small angles of incidence this approximation yields acceptable results, for larger angles of incidence it introduces numerical errors. Free surface and solid-solid boundary conditions can be implemented in numerical modeling with nonperiodic PS operators by using a boundary treatment based on characteristics variables (Kosloff et al., 1990; Kessler and Kosloff, 1991; Carcione, 1991; Tessmer et al., 1992; Igel, 1999). This method is proposed by Bayliss et al. (1986) to model free-surface and nonreflecting boundary conditions. The method can be summarized as follows (Tessmer et al., 1992; Carcione, 1994b). Consider the algorithm for the SH-wave equation (2). Most explicit time integration schemes compute the operation $\mathbf{Hv} \equiv (\mathbf{v})^{\text{old}}$, where $\mathbf{H}$ is defined in equation (2). The vector $(\mathbf{v})^{\text{old}}$ is then updated to give a new vector $(\mathbf{v})^{\text{new}}$ that takes the boundary conditions into account. Consider the boundary $x_3 = 0$ (e.g., the surface) and that the incident wave is incident on this boundary from the half-space $x_3 > 0$. Compute the eigenvalues of matrix $\mathbf{B}$: $\pm\sqrt{\mu/\rho} = \pm c$ and 0. Compute the right eigenvectors of matrix $\mathbf{B}$, such that they are the columns of a matrix $\mathbf{R}$, where $\mathbf{B} = \mathbf{R}\boldsymbol{\Lambda}\mathbf{R}^{-1}$, with $\boldsymbol{\Lambda}$ the diagonal matrix of the eigenvalues. If we define the characteristics vector as $\mathbf{c} = \mathbf{R}^{-1}\mathbf{v}$, and consider equation (2) corresponding to the modes traveling along the x_3-direction,

$$\frac{\partial \mathbf{c}}{\partial t} = \boldsymbol{\Lambda}\frac{\partial \mathbf{c}}{\partial x_3}, \tag{29}$$

the incoming and outgoing waves are decoupled. Two of the characteristic variables, components of vector $\mathbf{c}$ are $v_2 + \sigma_{32}/Z$ and $v_2 - \sigma_{32}/Z$, with $Z = \rho c$. The first variable is the incoming wave and the second variable is the outgoing wave. Equating the new and old outgoing characteristic and assuming stress-free boundary conditions ($\sigma_{32} = 0$), the update of the free- surface grid points is

$$\begin{pmatrix} v \\ \sigma_{12} \\ \sigma_{32} \end{pmatrix}^{\text{new}} = \begin{pmatrix} 1 & 0 & Z^{-1} \\ 0 & 1 & 0 \\ 0 & 0 & 0 \end{pmatrix} \begin{pmatrix} v \\ \sigma_{12} \\ \sigma_{32} \end{pmatrix}^{\text{old}}. \tag{30}$$

It can be shown that this application of the method of characteristics is equivalent to a paraxial approximation (Clayton and Engquist, 1977) in one spatial dimension.

Robertsson (1996) presents a FD method which does not rely on mapping transformations and therefore can handle arbitrary topography, although with a staircase shape. The free-surface condition is based on the method of images introduced by Levander (1988). This method is accurate and stable for high values of the Poisson ratio. An efficient solution to the staircase problem is given by Moczo et al. (1997), who propose a hybrid scheme based on the discrete-wavenumber, FD, and FE methods. These modeling algorithms include attenuation based on memory-variable equations (Emmerich and Korn, 1987; Carcione et al., 1988; Carcione, 1994b; Robertsson et al., 1994).

Interface boundary conditions are satisfied explicitly in homogeneous modeling (Kelly et al., 1976). At the interface

between a solid and a fluid, the normal particle velocity (or displacement, depending on the formulation) and normal stress components are continuous when crossing the interface; in a solid/solid boundary, both horizontal and vertical particle velocity components and normal stresses are continuous. However, heterogeneous modeling is preferred when the interfaces have arbitrary shape. In this case, spurious diffractions arise from an inappropriate modeling of curved and dipping interfaces (the so-called staircase effect). Irregular interfaces and variable grid spacing are easily handled by FE methods, since, in principle, grid cells can have any arbitrary shape. When using FD and PS algorithms, an averaging method can be used to reduce spurious diffractions arising from the staircase effect. Muir et al. (1992) used effective media theory based on Backus averaging to find the elastic constants at the four grid points of the cell. The modeling then requires an anisotropic stress-strain relation. Zeng and West (1996) obtain satisfactory results with a spatially weighted averaging of the model properties (slowness averaging, mainly), and Zhang and LeVeque (1997) present a method based on the modification of the FD scheme in the vicinity of an interface to satisfy the boundary conditions. Similarly, algorithms based on rectangular cells of varying size allow the reduction of staircase diffractions and the number of grid points (Moczo, 1989; Opršal and Zahradnik, 1999). When the grid points are not chosen in a geometrically regular way, combinations of 1-D Taylor series cannot be used, and 2-D Taylor series must be applied (Celia and Gray, 1992, 93).

Absorbing boundaries

The boundaries of the numerical mesh may produce nonphysical artifacts which disturb the physical events. These artifacts are reflections from the boundaries or wraparound as in the case of the Fourier method. The two main techniques used in seismic exploration and seismology to avoid these artifacts are the sponge method and the method based on the paraxial approximation.

The classical sponge method uses a viscous boundary or a strip along the boundaries of the numerical mesh, where the field is attenuated (Cerjan et al., 1985; Kosloff and Kosloff, 1986). When we consider the pressure formulation, equation (1) can be written as a system of coupled equations and modified as

$$\frac{\partial}{\partial t}\begin{pmatrix} p \\ q \end{pmatrix} = \begin{pmatrix} -\gamma & 1 \\ -L^2 & -\gamma \end{pmatrix}\begin{pmatrix} p \\ q \end{pmatrix} + \begin{pmatrix} 0 \\ f \end{pmatrix}, \tag{31}$$

where γ is an absorbing parameter. The solution to this equation is a wave traveling without dispersion but whose amplitude decreases with distance at a frequency-independent rate. A traveling pulse will thus diminish in amplitude without a change of shape. In the frequency domain, this implies that the stiffness is divided by the factor $i\omega+\gamma$, whereas the density is multiplied with the same factor. Therefore, the acoustic impedance remains real valued. This can be adjusted in such a way that the reflection coefficient is zero at the onset of the absorbing strip. An improved version of the sponge method is the perfectly matched-layer method or PML method used in electromagnetism (Berenger, 1994) and interpreted by Chew and Liu (1996) as a coordinate stretching. It is based on a (nonphysical) modification of the wave equation inside the absorbing strips, such that the reflection coefficient at the strip/model boundary is zero, and there is a free parameter to attenuate the wavefield. The improvement implies a reduction of nearly 75% in the strip thickness compared to the classical method.

The sponge method can be implemented in FE modeling by including a damping matrix $\mathbf{C}$ in equation (19):

$$\mathbf{KP} + \mathbf{C}\frac{\partial \mathbf{P}}{\partial t} + \mathbf{M}\frac{\partial^2 \mathbf{P}}{\partial t^2} + \mathbf{S} = 0, \tag{32}$$

with $\mathbf{C} = \alpha\mathbf{M} + \beta\mathbf{K}$, where α and β are the damping parameters (e.g., Sarma et al., 1998).

For approximations based on the one-way wave equation (paraxial) concept, consider the acoustic wave equation on the domain $x \geq 0$. At the boundary $x = 0$, the absorbing boundary condition has the general form

$$\left\{ \prod_{j=1}^{\mathrm{J}} \left[(\cos\alpha_j)\frac{\partial}{\partial t} - c\frac{\partial}{\partial x} \right] \right\} p = 0, \tag{33}$$

where $|\alpha_j| < \pi/2$ for all j (Higdon, 1991). Equation (33) provides a general representation of absorbing boundary conditions (Keys, 1985; Randall, 1988). The reason for the success of equation (33) is the following. Suppose that a plane wave is hitting the boundary at an angle α and a velocity c. In 2-D space, such a wave can be written as $p(x_1\cos\alpha + x_3\sin\alpha + ct)$. When an operator of the form $(\cos\alpha)\partial_{,t} - c\partial_{,x_1}$ is applied to this plane wave, the result is zero. The angles α_j are chosen to take advantage of a priori information about directions from which waves are expected to reach the boundary.

Consider now the approach based on characteristic variables (discussed in the "Boundary conditions" section) and apply it to the SH-wave equation (2) in the plane $x_3 = 0$. The outgoing characteristic variable is $v_2 - \sigma_{32}/Z$. This mode is left unchanged (new = old), while the incoming variable $v_2 + \sigma_{32}/Z$ is set to zero (new = 0). Then, the update of the boundary grid points is

$$\begin{pmatrix} v \\ \sigma_{12} \\ \sigma_{32} \end{pmatrix}^{\text{new}} = \frac{1}{2}\begin{pmatrix} 1 & 0 & Z^{-1} \\ 0 & 2 & 0 \\ Z & 0 & 1 \end{pmatrix}\begin{pmatrix} v \\ \sigma_{12} \\ \sigma_{32} \end{pmatrix}^{\text{old}}. \tag{34}$$

These equations are exact in one dimension (i.e., for waves incident at right angles). Approximations for the 2-D case are provided by Clayton and Engquist (1977).

Example

Modeling synthetic seismograms may have different purposes, for example, to design a seismic experiment (Özdenvar et al., 1996), to provide for structural interpretation (Fagin, 1992), or to perform a sensitivity analysis related to the detectability of a petrophysical variable, such as porosity, fluid type, fluid saturation, etc. Modeling algorithms can also be part of inversion and migration algorithms.

Model and modeling design

Designing a model requires the joint collaboration of geologists, geophysicists, and log analysts when there is well information of the study area. The geological modeling procedure generally involves the generation of a seismic-coherence volume to define the main reservoir units and the incorporation of

fault data of the study area. Seismic data require the standard processing sequence and prestack depth migration supported by proper inversion algorithms when possible. A further improvement is achieved by including well-logging (sonic- and density-log) information. Since the logs have a high degree of detail, averaging methods are used to obtain the velocity and density field at the levels of seismic resolution.

In planning the modeling with direct methods, the following steps should be followed.

1) From the maximum source frequency and minimum velocity, find the constraint on the grid spacing:
$$dx \le \frac{c_{\min}}{2 f_{\max}}. \tag{35}$$
This implies that the spacing should not exceed half the smallest wavelength in order to avoid aliasing. The actual grid spacing depends on the scheme chosen. For instance, an FD scheme which is second-order in time and fourth-order in space would require 5–8 grid points per minimum wavelength.
2) Find the number of grid points from the size of the model.
3) Allocate additional grid points for each absorbing strip at the sides, top, and bottom of the model. For instance, the standard sponge method requires four wavelengths, where the wavelength is given by $\lambda = 2c_{\max}/f_d$ and f_d is the dominant frequency of the seismic signal.
4) Choose the time step according to the stability condition (12) and accuracy criteria. Moreover, when possible, the modeling algorithm used requires testing against known analytical solutions to verify its correctness.
5) Define the source-receiver configuration.

Simulation

The 2-D model we consider is shown in Figure 2 with the properties indicated in Table 1. The low velocities and low quality factors of medium 7 simulate a sandstone subjected to an excess pore pressure. All the media have a Poisson ratio equal to 0.2, except medium 7 which has a Poisson ratio of 0.3, corresponding to an overpressure condition. The 2-D modeling algorithm (Carcione, 1992) is based on a fourth-order Runge-Kutta time-integration scheme and the Fourier and Chebyshev methods to compute the spatial derivatives along the horizontal and vertical directions, respectively. This allows the modeling of free-surface boundary conditions. Since the mesh is coarse (two points per minimum wavelength), Zeng and West's (1996) averaging method is applied to the slownesses to avoid diffractions due to the "staircase" effect (the density and the relaxation times are arithmetically averaged). The mesh has 135×129 points, with a horizontal grid spacing of 20 m and a vertical dimension of 2181 m with a maximum vertical grid spacing of 20 m. Stress-free and nonreflecting boundary conditions of the type of equations (30) and (34) are applied at the top and bottom boundaries, respectively. In addition, absorbing boundaries of the type of equation (31) with a length of 18 grid points are implemented at the sides and bottom boundary. The source is a vertical force (a Ricker wavelet) applied at 30-m depth with a maximum frequency of 40 Hz. The wavefield is computed by using a time step of 1 ms with a maximum time of 1 s (the total wall-clock time is 120 s for an Origin 2000 computer with four CPUs).

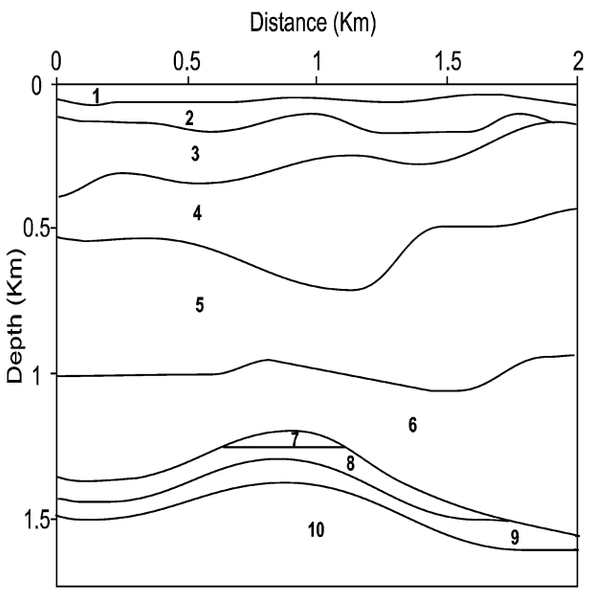

FIG. 2. Geological model. See Table 1 for material properties.

The seismogram recorded at the surface is shown in Figure 3, where the main event is the Rayleigh wave (ground roll) traveling with wave velocities between the shear velocities of media 1 and 2, approximately. The reflection event corresponding to the anticlinal structure can be clearly seen between 0.6 and 0.8 s.

INTEGRAL-EQUATION METHODS: HUYGENS' PRINCIPLE

As a first step in discussing integral-equation methods, let us consider Huygens' formulation illustrated in Figure 1. Huygens states that the wavefield originating from the flame can be considered as a superposition of waves due to point sources located in the flame. We can also formulate this in a somewhat more mathematical way. Consider the scalar wave equation for a homogeneous medium (i.e., with constant density and constant speed of sound $c = c_0$),
$$\left(\nabla \cdot \nabla - \frac{1}{c_0^2}\frac{\partial^2}{\partial t^2}\right) p = -q, \tag{36}$$

Table 1. Material properties for the geological model in Figure 2.

Medium	V_P (km/s)	V_S (km/s)	Q_P	Q_S	ρ g/cm^3
1	2.6	1.6	80	60	2.1
2	3.2	1.96	100	78	2.3
3	3.7	2.26	110	85	2.3
4	4	2.45	115	90	2.4
5	4.3	2.63	120	92	2.5
6	4.5	2.75	125	95	2.6
7	3.2	1.7	30	25	2.3
8	4.6	2.82	150	115	2.6
9	4.8	2.94	160	120	2.7
10	5.4	3.3	220	170	2.8

which follows from equation (1) with $q = c_0^{-2} f$. The integral representation for this scalar wave equation is given by (Courant and Hilbert, 1937, 403)

$$p(\mathbf{x}, t) = \int G(\mathbf{x}, \mathbf{x}_s, t - t')\, q(\mathbf{x}_s, t')\, d\mathbf{x}_s\, dt', \qquad (37)$$

where $\mathbf{x}$ is the position vector. Since the velocity is constant, the Green's function G is given by

$$G(\mathbf{x}, \mathbf{x}_s, t) = \frac{\delta(t - |\mathbf{x} - \mathbf{x}_s|/c_0)}{4\pi |\mathbf{x} - \mathbf{x}_s|}. \qquad (38)$$

The Green's function is the medium's response to a point source, and satisfies the wave equation (36) for a point source given by $q = \delta(\mathbf{x} - \mathbf{x}_s)\delta(t)$. If we substitute equation (38) into equation (37), we obtain the integral representation

$$p(\mathbf{x}, t) = \int_D \frac{q(\mathbf{x}_s, t - |\mathbf{x} - \mathbf{x}_s|/c_0)}{4\pi |\mathbf{x} - \mathbf{x}_s|}\, d\mathbf{x}_s, \qquad (39)$$

where D is the region in space where the source term q is present. Equation (39) is the mathematical formulation of Huygens' principle illustrated in Figure 1. The integration is a summation over volumetric wave field densities, $q/4\pi|\mathbf{x} - \mathbf{x}_s|$. Each element of that distribution resides at a "source point" $\mathbf{x}_s$ at time t and arrives at the point $\mathbf{x}$ at the retarded time $t - |\mathbf{x} - \mathbf{x}_s|/c_0$. The volumetric wave field density is given by the initial source distribution, q, weighted by the so-called "3-D spreading factor" $4\pi|\mathbf{x} - \mathbf{x}_s|$. In order to derive the wave equation and its corresponding integral representation above, one needs integral and differential calculus which was not yet developed at the time of Huygens.

Domain integral-equation method

Apart from radiation from sources, as illustrated by equation (39), domain-integral representations can also be used to formulate and solve scattering problems. Consider, for instance, the case of a scattering object V with a sound speed $c(\mathbf{x})$ embedded in a surrounding medium with constant sound speed c_0. Both scattering object and embedding medium have the same (constant) density ρ_0. The wave equation then reads,

$$\left(\nabla \cdot \nabla - \frac{1}{c^2}\frac{\partial^2}{\partial t^2}\right) p = -q, \qquad (40)$$

with $c = c_0$ outside V. This can be rewritten in the following contrast formulation:

$$\left(\nabla \cdot \nabla - \frac{1}{c_0^2}\frac{\partial^2}{\partial t^2}\right) p = -q - \left(\frac{1}{c_0^2} - \frac{1}{c^2}\right)\frac{\partial^2 p}{\partial t^2}. \qquad (41)$$

The wave equation we obtain in this way is very similar to equation (36), the only difference being an additional source term due to the presence of the object. Therefore, we can write the integral representation, analogous to equation (39), in the form

$$p = p^{inc} + p^{sc}, \qquad (42)$$

where the incident field p^{inc}, which would have been present due to the source q in the absence of the object, is given by the right-hand side of equation (39) and the scattered field is given by

$$p^{sc}(\mathbf{x}, t) = \int_V \left(\frac{1}{c_0^2} - \frac{1}{c(\mathbf{x}')^2}\right)\frac{\partial^2}{\partial t^2}\frac{p(\mathbf{x}', t - R/c_0)}{4\pi R}\, d\mathbf{x}', \qquad (43)$$

with $R = |\mathbf{x} - \mathbf{x}'|$ the distance between observation point $\mathbf{x}$ and integration point $\mathbf{x}'$. With the aid of equations (42)–(43), the field outside the object V can be represented in terms of the sources q and the field values inside the object. In order to determine the field values inside the object, we can take $\mathbf{x}$ inside V in equation (42), substitute p^{sc} of equation (43), and obtain an integro-differential equation for the unknown field p inside the object V. So far, the acoustic case has been presented here for the sake of simplicity. The elastic case has been discussed by Pao and Varatharajulu (1976). For an overview of different methods for acoustic, electromagnetic, and elastic fields, see De Hoop (1995).

In the above, a homogeneous embedding medium was considered. This method is also applicable to heterogeneous embedding media, provided the Green's function (the wavefield due to a point source) can be determined. This is the case for layered media using plane-wave summation techniques (Ursin, 1983).

For special geometries, the volume integral equation obtained here can be solved with the aid of separation techniques. In general, however, these methods are not applicable and the equation has to be solved numerically. This can be done with the method of moments (Harrington, 1968). The first step in applying this method is discretization of the unknown function with the aid of expansion functions, followed by a weighting of the integral equation using appropriate weighting functions. To illustrate this procedure, we apply it to the integral-equation formulation given by equations (42)–(43). First, we subdivide the volume V of the scatterer into smaller volumes V^m with centers $\mathbf{x}^m (m = 1, \ldots M)$ and assume that the pressure is constant in each subvolume. If we then enforce the equality sign at

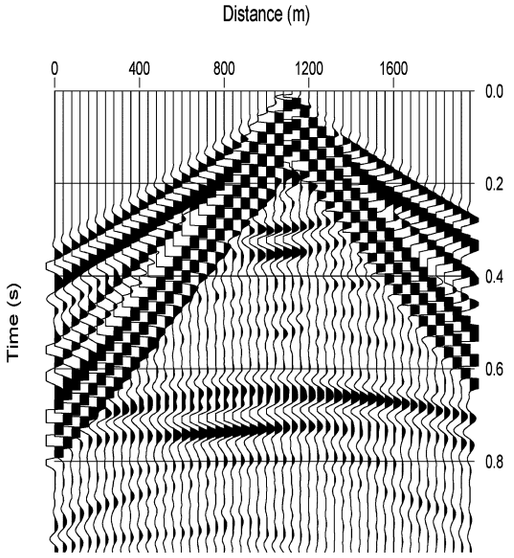

FIG. 3. Seismogram of the vertical particle velocity.

the center points at times t_j, we obtain the following relation:

$$p(\mathbf{x}^n, t_j) = p^{inc}(\mathbf{x}^n, t_j) + \sum_{m=1}^{M} \int_{V^m} \left(\frac{1}{c_0^2} - \frac{1}{c(\mathbf{x}')^2} \right) \times \frac{\partial_t^2 p(\mathbf{x}', t_j - R^n/c_0)}{4\pi R^n} \, d\mathbf{x}', \quad (44)$$

with $n = 1, 2, \ldots M$ and R^n the distance between $\mathbf{x}^n$ and $\mathbf{x}'$. If we express the time derivative under the integral in backward time differences, we obtain an explicit time-stepping algorithm where new values in each point can be computed from previously computed values. In this way, no matrix inversion is required. A disadvantage of this method, however, is that one has to be aware of potential instabilities and that previously computed values in all points have to be stored. If the object is large compared to the pulse width of the field, this approach becomes impractical. An alternative is to formulate the problem in the frequency domain and solve the resulting system of equations separately for each frequency. This circumvents the storage and stability problems but can still be inefficient if the object is large compared to the wavelength due to the fact that the system matrix is full (in contrast to FD methods). Therefore, this type of volume integral-equations is especially suited to the case of objects of modest size.

Boundary integral-equation methods

In Figure 4, Huygens' principle is illustrated in a different form. Each point on a wavefront can be considered as the source of waves propagating away from that point. In order to obtain a mathematical formulation corresponding to the situation of Figure 4, we again consider the wave equation, but this time in a domain D containing a bounded object with boundary S (D is the region outside S). On S, we prescribe an explicit boundary condition, for example a pressure-release boundary condition. We then have the following relations:

$$\left(\nabla \cdot \nabla - \frac{1}{c_0^2} \frac{\partial^2}{\partial t^2} \right) p(\mathbf{x}, t) = -q(\mathbf{x}, t), \quad (\mathbf{x} \in D), \quad (45)$$

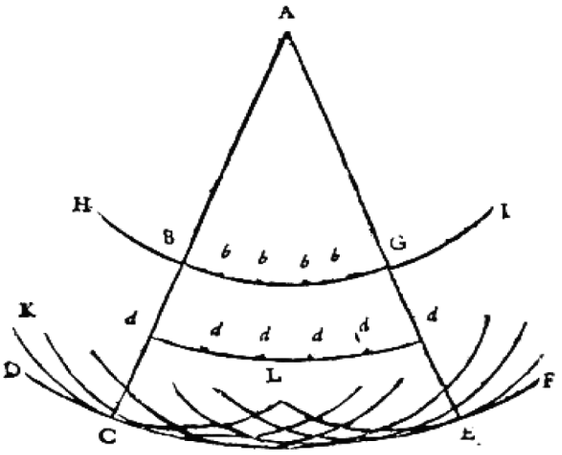

FIG. 4. Illustration of Huygens' principle showing that each point on a wavefront acts as secondary source for spherical waves [taken from the 1690 *Traité de la lumière* (Huygens, 1990)].

and boundary condition

$$p(\mathbf{x}, t) = 0 \quad (\mathbf{x} \in S). \quad (46)$$

As in the previous section, the pressure in D can now be decomposed into two contributions,

$$p = p^{inc} + p^{sc}, \quad (47)$$

where the incident field, p^{inc}, is again given by the right-hand side of equation (39), and the scattered field, accounting for the presence of the object, is given by the integral representation

$$p^{sc}(\mathbf{x}, t) = \int_S \frac{\mathbf{n} \cdot \nabla' p(\mathbf{x}', t - R/c_0)}{4\pi R} \, d\mathbf{x}', \quad (48)$$

where $\mathbf{n}$ is the outward pointing normal vector on S. This can be derived by applying the boundary condition (46) to the integral representation for the scalar wave equation in a bounded domain (see, for instance, Bennett and Mieras, 1981). The integration over S is in fact a summation of point-source wavefields located on S and is therefore a mathematical representation of the same idea illustrated in Figure 4. With the aid of equations (47)–(48), the field ouside the object can be represented in terms of sources q and certain field values at the boundary of the object. In order to determine these field values, we can let the point of observation approach the object and enforce the boundary condition (46). In this way, we obtain the integral equation

$$p^{inc}(\mathbf{x}, t) = -\int_S \frac{\mathbf{n} \cdot \nabla' p(\mathbf{x}', t - R/c_0)}{4\pi R} \, d\mathbf{x}' \quad (\mathbf{x} \in S). \quad (49)$$

From this equation, the field quantity $\mathbf{n} \cdot \nabla' p$ on S can be determined. In general, this integral equation has to be solved numerically using methods similar to those discussed for the case of the volume-integral equation. In the discretization procedure, proper care has to be taken of the singularity of the Green's function at $\mathbf{x} = \mathbf{x}'$. Here, we have only discussed a scalar example for the pressure-release boundary condition. The elastic formulation for the above problem is given by Tan (1976). Scattering of elastic waves by cracks or cavities has also been discussed by Bouchon (1987) and, more recently, elastic scattering by hydrofractures was discussed by Pointer et al. (1998). The application of integral-equation techniques for studying wave propagation in media with a number of cracks was discussed by Liu et al. (1997), whereas wave propagation in media containing large numbers (several thousands) of small cracks was studied by Muijres et al. (1998). In particular, the case of many small cracks can be solved very efficiently with the aid of boundary-integral equations since each crack is represented by only one unknown coefficient which represents the jump in normal velocity.

Boundary-integral equations are also very well suited to accurately model geometries with either explicit boundary conditions or discontinuities in properties. For instance, scattering of elastic waves by a rough interface between two solids was discussed by Fokkema (1980). The geometry of irregular boreholes was considered by Bouchon and Schmidt (1989), and the radiation of seismic sources in boreholes in layered and anisotropic media was discussed by Dong et al. (1995).

Integral-equation modeling example

In order to investigate the effect of small-scale scattering objects like cracks or inclusions, integral equations can be useful. If the cracks are small with respect to the dominant seismic wave length, each crack only adds one unknown to the problem, which implies that large number of cracks can be modeled. In Figure 5, 4000 cracks are randomly positioned in a homogeneous embedding medium with sound velocity $c_0 = 3000$ m/s. After choosing the wave form of the incident pressure field (in the frequency domain) and solving the relevant integral equation numerically for each frequency, the resulting total transmitted field at the receiver is shown in Figure 6 in comparison with the incident field. This method is described in more detail in Muijres et al. (1998).

ASYMPTOTIC (RAY-TRACING) METHODS

The integral representations discussed in the previous section are especially useful if the medium is homogeneous. In the case of heterogeneous media, the computation of the Green's function is tedious. In that case, asymptotic methods can be an attractive alternative. Before we discuss the asymptotic methods, we first return to equation (38), the Green's function for a homogeneous medium. Clearly, this function describes a spherical wavefront which propagates at speed c_0. An initial disturbance of the medium at $t = 0$ and $\mathbf{x} = \mathbf{x}_s$ is spreading in space as time proceeds; at time t, it has arrived at the sphere $|\mathbf{x} - \mathbf{x}_s| = c_0 t$. The function

$$\phi(\mathbf{x}, \mathbf{x}_s) = |\mathbf{x} - \mathbf{x}_s|/c_0 \tag{50}$$

measures the time needed for the disturbance to travel from the source location $\mathbf{x}_s$ to the point $\mathbf{x}$. It is called the traveltime function. The *amplitude* of the disturbance is given by the function

$$A(\mathbf{x}, \mathbf{x}_s) = \frac{1}{4\pi|\mathbf{x} - \mathbf{x}_s|}. \tag{51}$$

With these two definitions, we can rewrite the Green's function for a constant velocity medium as

$$G(\mathbf{x}, \mathbf{x}_s, t) = A(\mathbf{x}, \mathbf{x}_s)\delta(t - \phi(\mathbf{x}, \mathbf{x}_s)). \tag{52}$$

In what follows, we work with the temporal Fourier transform of the Green's function, which is denoted by $G(\mathbf{x}, \mathbf{x}_s, \omega)$. For the constant velocity case, it is of the form

$$G(\mathbf{x}, \mathbf{x}_s, \omega) = A(\mathbf{x}, \mathbf{x}_s)\mathrm{e}^{i\omega\phi(\mathbf{x}, \mathbf{x}_s)}. \tag{53}$$

In general, the velocity of course varies with position $\mathbf{x}$. In geophysical applications, this is predominantly caused by transitions from one geological formation to another, but there are also other causes, such as varying geopressure or fluid content of the rocks. From physical intuition, one would expect that the solution of the wave equation (36) still behaves like a propagating wavefront in this case. This can be made more precise mathematically by studying the high frequency behavior of $G(\mathbf{x}, \mathbf{x}_s, \omega)$. It can be shown that in the limit $\omega \to \infty$ (hence the name asymptotic) $G(\mathbf{x}, \mathbf{x}_s, \omega)$ is still of the form of equation (53), where $\phi(\mathbf{x}, \mathbf{x}_s)$ and $A(\mathbf{x}, \mathbf{x}_s)$ are general traveltime and amplitude functions. The wavefront is no longer spherical in the heterogeneous case, and the traveltime and amplitude functions are no longer given by the simple explicit relations (50) and (51) above.

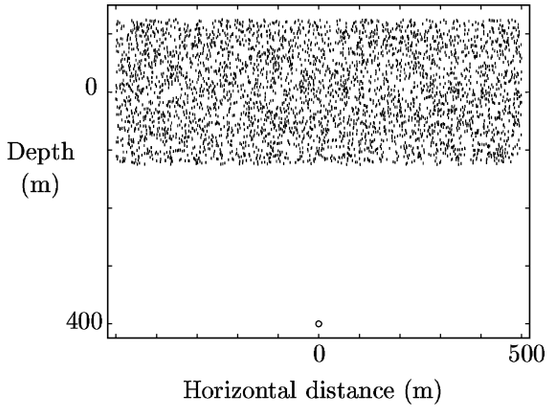

FIG. 5. Model consisting of 4000 cracks having a width of 1 m each. The speed of sound in the embedding medium is 3000 m/s. The receiver location is indicated with o; the incident wave is a plane pressure wave propagating downwards.

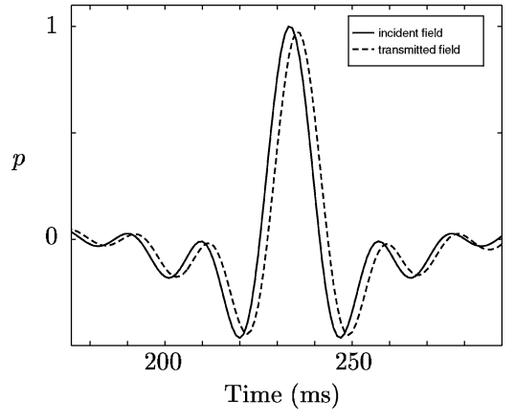

FIG. 6. Normalized incident pressure field recorded by the receiver in the absence of cracks and transmitted total field accounting for the presence of the cracks.

Eikonal and transport equations

We illustrate the use of asymptotic methods by constructing the high-frequency behavior of the Green's function $G(\mathbf{x}, \mathbf{x}_s, \omega)$ away from the location of the source (i.e., for $\mathbf{x} \neq \mathbf{x}_s$). We start by substituting the expression (53) into the Fourier transform of the wave equation. This equation is given by

$$\left(\nabla \cdot \nabla - \frac{(-i\omega)^2}{c(\mathbf{x})^2}\right) G(\mathbf{x}, \mathbf{x}_s, \omega) = 0 \tag{54}$$

and is known as the Helmholtz equation. The result is

$$((i\omega)^2[(\nabla\phi)^2 - c^{-2}(\mathbf{x})]A + i\omega[2\nabla A \cdot \nabla\phi + A\Delta\phi] + \Delta A)e^{i\omega\phi} = 0. \tag{55}$$

Dividing out the factor $e^{i\omega\phi}$, we obtain a polynomial in $i\omega$, which is equated to zero. Since this equation has to hold for all ω, all the coefficients of the polynomial have to be zero.

From the coefficient of $(i\omega)^2$, we find that the traveltime function has to satisfy the so-called eikonal equation

$$(\nabla\phi)^2 = c^{-2}(\mathbf{x}). \tag{56}$$

Similarly, from the coefficient of $i\omega$ we find

$$2\nabla A \cdot \nabla\phi + A\Delta\phi = 0. \tag{57}$$

This equation is called the transport equation for the amplitude function. These two equations, when supplemented with suitable initial conditions, determine the traveltime and amplitude function uniquely. For a constant velocity, this leads to an amplitude given by equation (51) for which $\Delta A = 0$. For spatially varying velocity, $\Delta A \neq 0$, which implies that the coefficient of $(i\omega)^0$ in equation (55) is not equal to zero. Therefore, one is forced to replace the simple solution (53) by a power series in $(-i\omega)^{-1}$, i.e.,

$$G(\mathbf{x}, \mathbf{x}_s, \omega) = \sum_{k\geq 0}(-i\omega)^{-k} A_k(\mathbf{x}, \mathbf{x}_s) e^{i\omega\phi(\mathbf{x},\mathbf{x}_s)}. \tag{58}$$

To determine the equations for the higher order amplitudes A_{k+1} $(k \geq 0)$, one substitutes this expression in the Helmholtz equation and equates the coefficients of all powers of ω to zero. Besides the eikonal equation (56) for $\phi(\mathbf{x}, \mathbf{x}_s)$ and the transport equation (57) for $A_0(\mathbf{x}, \mathbf{x}_s)$, one finds for $k \geq 0$ the following higher order transport equations:

$$2\nabla A_{k+1} \cdot \nabla\phi + A_{k+1}\Delta\phi = \Delta A_k. \tag{59}$$

This shows that a solution of the wave equation of the form (58) can be constructed by first solving the eikonal equation for $\phi(\mathbf{x}, \mathbf{x}_s)$, subsequently the transport equation for $A_0(\mathbf{x}, \mathbf{x}_s)$, and then solving the higher order transport equations recursively for $A_{k+1}(\mathbf{x}, \mathbf{x}_s)$ $(k \geq 0)$.

So we are naturally led to an infinite power series (58) in $1/\omega$, which converges for $|\omega| \geq \omega_0 \geq 0$. If $\omega_0 = 0$, it converges for all frequencies; if $\omega_0 = \infty$, the series is meaningless. If the series converges uniformly in $\mathbf{x}$ for a given frequency, it is a solution of the Helmholtz equation for that frequency. The fact that the series (58) in general diverges for small frequencies means that we have only constructed the solution of the Helmholtz equation for large frequencies. Therefore, ones speaks of an asymptotic solution of the Helmholtz equation.

Let us try to assess the consequence of knowing only a high-frequency solution for the time-domain solution. To this end, we take the inverse Fourier transform of $G(\mathbf{x}, \mathbf{x}_s, \omega)$, which can be written as

$$G(\mathbf{x}, \mathbf{x}_s, t) = \frac{1}{2\pi}\int_{-\omega_0}^{\omega_0} G(\mathbf{x}, \mathbf{x}_s, \omega) e^{-i\omega t}\, d\omega + \frac{1}{2\pi}\int_{|\omega|>\omega_0} G(\mathbf{x}, \mathbf{x}_s, \omega) e^{-i\omega t}\, d\omega. \tag{60}$$

The first term is not known (at least not by the procedure outlined above) unless ω_0 happens to be zero. The only thing that can be said about it is that it must be a smooth function of t, $\mathbf{x}$ and $\mathbf{x}_s$, since differentiation can be done under the integral for an integral over a finite interval. Equivalently, the second term of equation (60) is representative for the singular (i.e., nonsmooth) behavior of the solution. The smooth part of the solution has a frequency dependence that must decay faster than any algebraic power of ω and can therefore not be represented by a power series.

If $\hat{w}(\omega)$ is a smooth taper function satisfying, e.g.,

$$\hat{w}(\omega) = \begin{cases} 0 & \text{if } |\omega| \leq \omega_0 \\ 1 & \text{if } |\omega| \geq 2\omega_0, \end{cases} \tag{61}$$

we can write

$$G(\mathbf{x}, \mathbf{x}_s, t) \sim \frac{1}{2\pi}\int \hat{w}(\omega) G(\mathbf{x}, \mathbf{x}_s, \omega) e^{-i\omega t}\, d\omega, \tag{62}$$

where the $\sim$ sign means that we have neglected a smooth function. The taper function effectively acts as a high-pass filter. We can now substitute the series (58) in the right-hand side of this relation. The term with $k = 0$ transforms into $A_0 w(t - \phi)$ [which equals $A_0\,(w * \delta_\phi)(t)$, a high-pass version of a propagating wavefront]. Similarly, the term with $k = 1$ transforms into $A_1\,(w * H_\phi)(t)$, where H is the Heaviside step function, given by

$$H_a(t) = \begin{cases} 0 & \text{if } t < a \\ 1 & \text{if } t \geq a. \end{cases} \tag{63}$$

This is again a propagating wavefront. The Heaviside function is discontinuous at the wavefront $\phi(\mathbf{x}, \mathbf{x}_s) = t$, but the discontinuity of the Heaviside function is of course less severe than the singularity of the delta function. Similarly, the higher order terms, which can be obtained by repeatedly integrating with respect to t, become less and less singular.

Usually, one breaks off the solution after the first term. From the above, it is clear that this means that one only considers the most singular part of the solution. Moreover, for the constant velocity case, the first term coincides with the full solution.

Constructing the asymptotic solution

Before discussing numerical methods, we first explain how to construct a solution from a theoretical point of view by the method of characteristics. Numerical methods for solving the eikonal and transport equations rely heavily on this theoretical concept.

Method of characteristics: seismic rays

The method of characteristics is in fact a general solution method for first-order partial differential equations, of which the eikonal equation is an example [see, e.g., Courant and Hilbert (1966) for a classical reference]. The general idea is to construct curves $\mathbf{x}(\sigma)$ along which the partial differential equation reduces to an ordinary differential equation.

To explain this concept in the case of the eikonal equation, we again first consider the simplest case of a constant velocity. In that case the wavefronts (i.e., the surfaces of constant traveltime t) are spheres of radius ct centered at the source location $\mathbf{x}_s$ [see equation (50)]. Moreover, choosing an arbitrary point $\mathbf{x}$ on a wavefront $\phi = t$, the line from $\mathbf{x}_s$ to $\mathbf{x}$ is orthogonal to that wavefront and hence in the direction of the gradient $\nabla\phi(\mathbf{x}, \mathbf{x}_s)$. Therefore, this line can be parameterized as

$$\mathbf{x}(\sigma) = \mathbf{x}_s + \sigma\nabla\phi(\mathbf{x}, \mathbf{x}_s) = \mathbf{x}_s + \frac{\sigma}{c}\frac{\mathbf{x} - \mathbf{x}_s}{|\mathbf{x} - \mathbf{x}_s|}, \tag{64}$$

where we have scaled the parameter σ in such a way that

$$\frac{d\mathbf{x}}{d\sigma} = \nabla\phi = \frac{1}{c}\frac{\mathbf{x}-\mathbf{x}_s}{|\mathbf{x}-\mathbf{x}_s|}. \tag{65}$$

Differentiating the traveltime function $\phi(\mathbf{x}, \mathbf{x}_s)$ along this line $\mathbf{x}(\sigma)$, we obtain

$$\frac{d\phi}{d\sigma} = \frac{d\mathbf{x}}{d\sigma}\cdot\nabla\phi = (\nabla\phi)^2 = \frac{1}{c^2}, \tag{66}$$

which is indeed an ordinary differential equation for the traveltime. Given the line and this equation, the traveltime function is easily retrieved. Integrating with respect to σ, one finds $\phi = \sigma/c^2$. Moreover, from equation (64) one finds that $\sigma = c|\mathbf{x}-\mathbf{x}_s|$, and hence $\phi(\mathbf{x}, \mathbf{x}_s) = |\mathbf{x}-\mathbf{x}_s|/c$.

In conclusion, we can say that, for the constant velocity case, it is sufficient to have the family of lines originating from the source location (these are the characteristic curves in this case) and the ordinary differential equation (66) along these lines to solve for the traveltime function.

In the general case of a spatially varying velocity, we would also like to construct curves $\mathbf{x}(\sigma)$ satisfying $d\mathbf{x}/d\sigma = \nabla\phi$. Unfortunately, to construct these curves, one would have to know the solution ϕ of the eikonal equation up front, whereas the whole purpose of constructing characteristics is to find this solution. To circumvent this problem, we differentiate once more with respect to σ:

$$\begin{aligned}\frac{d^2\mathbf{x}}{d\sigma^2} &= \frac{d}{d\sigma}\nabla\phi\\ &= \frac{d\mathbf{x}}{d\sigma}\cdot\nabla(\nabla\phi)\\ &= \nabla\phi\cdot\nabla(\nabla\phi)\\ &= \nabla[(\nabla\phi)^2/2]\\ &= \nabla[c^{-2}/2].\end{aligned} \tag{67}$$

Hence, we find a second-order equation for the curve $\mathbf{x}(\sigma)$ which does not depend on the solution ϕ. This second-order equation is equivalent to the system of first-order equations

$$\begin{aligned}\frac{d\mathbf{x}}{d\sigma} &= \mathbf{p},\\ \frac{d\mathbf{p}}{d\sigma} &= \nabla[c^{-2}/2].\end{aligned} \tag{68}$$

The solution curves $(\mathbf{x}(\sigma), \mathbf{p}(\sigma))$ of this system are called bicharacteristic curves. They belong to the phase space $\{(\mathbf{x}, \mathbf{p}) \mid \mathbf{x}, \mathbf{p} \in \mathbf{R}^3\}$. The curves $\mathbf{x}(\sigma)$, which live in the configuration space $\mathbf{R}^3$, are called the characteristic curves or, briefly, the characteristics of the eikonal equation. In seismology, they are also referred to as (seismic) rays.

The system (68) can be solved if we specify initial conditions $\mathbf{x}(0)$ and $\mathbf{p}(0)$. We choose

$$\mathbf{x}(0) = \mathbf{x}_s, \qquad \mathbf{p}(0) = \frac{1}{c(\mathbf{x}_s)}\begin{pmatrix}\sin\xi_1\cos\xi_2\\ \sin\xi_1\sin\xi_2\\ \cos\xi_1\end{pmatrix}. \tag{69}$$

Thus, all rays start at $\mathbf{x}_s$ for $\sigma = 0$ and leave the source location in the direction specified by the angles ξ_1 and ξ_2. The solution curves depend smoothly on the initial conditions $\mathbf{x}_s$, ξ_1, and ξ_2.

If the source location is fixed, we write $\mathbf{x} = \mathbf{x}(\xi_1, \xi_2; \sigma)$ and $\mathbf{p} = \mathbf{p}(\xi_1, \xi_2; \sigma)$ to denote the dependence on the take-off angles of the ray at $\mathbf{x}_s$.

In fact, the solution curve $\mathbf{x}(\xi_1, \xi_2; \sigma)$ defines a map $(\xi_1, \xi_2, \sigma) \mapsto \mathbf{x}(\xi_1, \xi_2; \sigma)$ which can be seen as a coordinate transformation provided, of course, that the Jacobian

$$J(\xi_1, \xi_2, \sigma) = \frac{\partial(x, y, z)}{\partial(\xi_1, \xi_2, \sigma)} \tag{70}$$

does not vanish. Notice that for the constant velocity case, this is just the transformation from spherical to rectangular coordinates, and the Jacobian indeed does not vanish away from the source location.

In order to construct a solution $\phi(\mathbf{x}, \mathbf{x}_s)$ of the eikonal equation, we supplement (just as in the constant velocity case) the equations (68) with the equation

$$\frac{d\tilde{\phi}}{d\sigma} = \frac{1}{c^2}, \qquad \tilde{\phi}(0) = 0. \tag{71}$$

Integrating this equation along a characteristic curve $\mathbf{x}(\xi_1, \xi_2; \sigma)$, one finds

$$\tilde{\phi}(\xi_1, \xi_2; \sigma) = \int_0^\sigma \frac{d\sigma'}{c^2(\mathbf{x}(\xi_1, \xi_2; \sigma'))}. \tag{72}$$

If the Jacobian J introduced in equation (70) is indeed nonzero, this function can also be seen as a function of $\mathbf{x}$:

$$\phi(\mathbf{x}(\xi_1, \xi_2; \sigma), \mathbf{x}_s) = \tilde{\phi}(\xi_1, \xi_2; \sigma). \tag{73}$$

Notice that equation (68) is a system of Hamilton equations for the Hamiltonian H, given by

$$H(\mathbf{x}, \mathbf{p}) = (\mathbf{p}^2 - c^{-2}(\mathbf{x}))/2. \tag{74}$$

This system can be written as

$$\begin{aligned}\frac{d\mathbf{x}}{d\sigma} &= \frac{\partial H}{\partial \mathbf{p}},\\ \frac{d\mathbf{p}}{d\sigma} &= -\frac{\partial H}{\partial \mathbf{x}}.\end{aligned} \tag{75}$$

Let $\tilde{H}(\xi_1, \xi_2, \sigma) = H(\mathbf{x}(\xi_1, \xi_2; \sigma))$. Then, because of these equations, $\tilde{H}$ is independent of σ:

$$\frac{\partial\tilde{H}}{\partial\sigma} = \frac{d\mathbf{x}}{d\sigma}\cdot\frac{\partial H}{\partial\mathbf{x}} + \frac{d\mathbf{p}}{d\sigma}\cdot\frac{\partial H}{\partial\mathbf{p}} = 0. \tag{76}$$

Moreover, because of the initial conditions (69), $\tilde{H}(\xi_1, \xi_2, 0) = 0$. Therefore, the Hamiltonian vanishes identically along the bicharacteristics:

$$\tilde{H}(\xi_1, \xi_2, \sigma) = 0. \tag{77}$$

From the definition of H, we see that this means nothing else than that the length of the tangent vector $\mathbf{p}(\xi_1, \xi_2; \sigma) = d\mathbf{x}(\xi_1, \xi_2; \sigma)/d\sigma$ is always $1/c(\mathbf{x})$. For this reason, $\mathbf{p}$ is often called a slowness vector in geophysics.

The only thing left to show is that the function $\phi(\mathbf{x}, \mathbf{x}_s)$ that we have constructed in this way does indeed satisfy the eikonal equation. Since we have just shown that $\mathbf{p}^2 = c^{-2}$, it is sufficient to show that $\mathbf{p} = \nabla\phi$, just as in the constant velocity case. A proof of this relation can be found in Courant and Hilbert (1966).

Transport along the rays

Now let us turn our attention to the transport equation (57). This equation can also be rewritten as an ordinary differential equation along the rays. The gradient of the traveltime function in a point $\mathbf{x}(\xi_1, \xi_2; \sigma)$ is given by the momentum vector $\mathbf{p}(\xi_1, \xi_2; \sigma)$ which, according to Hamilton's equations (68), is equal to the tangent vector $d\mathbf{x}/d\sigma$. Therefore, the term $\nabla A \cdot \nabla\phi$ represents the derivative $dA/d\sigma$ of the amplitude along a ray. Hence, we can cast the transport equation into the form

$$\frac{1}{A}\frac{dA}{d\sigma} = -\frac{1}{2}\Delta\phi. \tag{78}$$

In fact, there is a simpler form of the transport equation which uses the identity

$$\Delta\phi = \frac{1}{J}\frac{dJ}{d\sigma}. \tag{79}$$

This follows from the definition (70) of the determinant J and Hamilton's equations (Červený et al., 1977; Červený, 1985, 1987). Using this identity, we find

$$\frac{d}{d\sigma}(\sqrt{J}A) = 0. \tag{80}$$

In other words, the quantity $\sqrt{J}A$ is equal to a constant C along a ray. The constant C can be found by requiring that the amplitude A approaches the constant velocity amplitude A given by equation (51) for $\sigma \downarrow 0$ [see, e.g., Bleistein (1984)]. The result is

$$C = \frac{1}{4\pi}\sqrt{\frac{\sin\xi_1}{c(\mathbf{x}_s)}}. \tag{81}$$

So we get

$$A(\mathbf{x}, \mathbf{x}_s) = \frac{1}{4\pi}\sqrt{\frac{\sin\xi_1}{c(\mathbf{x}_s)J(\xi_1, \xi_2; \sigma)}}. \tag{82}$$

This result shows that the amplitude of the Green's function can be calculated from the determinant of the matrix

$$Q = \left(\frac{\partial\mathbf{x}}{\partial\xi_1}, \frac{\partial\mathbf{x}}{\partial\xi_2}, \frac{\partial\mathbf{x}}{\partial\sigma}\right). \tag{83}$$

If we also introduce the matrix

$$P = \left(\frac{\partial\mathbf{p}}{\partial\xi_1}, \frac{\partial\mathbf{p}}{\partial\xi_2}, \frac{\partial\mathbf{p}}{\partial\sigma}\right), \tag{84}$$

we can derive from Hamilton's equations that the matrices Q and P satisfy the system of ordinary differential equations

$$\frac{dQ}{d\sigma} = P, \qquad \frac{dP}{d\sigma} = Q^t\nabla\nabla(c^{-2}/2). \tag{85}$$

Solving the Hamilton equations (68) together with the system (85) is called dynamic ray tracing [see, e.g., Červený et al. (1977) and Červený (1985, 1987) for a standard reference]. It enables us to calculate the traveltimes and amplitudes necessary for the computation of the asymptotic Green's function. The elements of the matrices Q and P are used in many asymptotic calculations, e.g., in true amplitude Kirchhoff migration [see, e.g., Bleistein et al. (2001) for a recent reference].

Caustics

In the previous section, we saw that the determinant $J(\xi_1, \xi_2, \sigma)$ defined in equation (70) plays an important role. If it is nonzero, the transformation $(\xi_1, \xi_2, \sigma) \mapsto (x_1, x_2, x_3)$ is a coordinate transformation, which enables us to consider the traveltime function ϕ in equation (72) and the amplitude function A in equation (82) as functions of (x_1, x_2, x_3) rather than of (ξ_1, ξ_2, σ). Moreover, J occurs explicitly in the expression (82) for the amplitude. A point $\mathbf{x}_0(\xi_1^{(0)}, \xi_2^{(0)}, \sigma^{(0)})$, for which $J(\xi_1^{(0)}, \xi_2^{(0)}, \sigma^{(0)})$ vanishes, is called a caustic point. From equation (82), it is clear that we are in serious trouble here, since the amplitude $A(x_0, x_s)$ would be infinite. Because of this, it is impossible to find a solution of the simple form $Ae^{i\omega\phi}$ for the Green's function at a caustic point.

Let us analyze from a geometrical point of view the vanishing of the determinant. To this end, we consider the collection of all solutions of the ray equations $\{\mathbf{x}(\xi_1, \xi_2; \sigma), \mathbf{p}(\xi_1, \xi_2; \sigma)\}$ in phase space, the 6-D space spanned by all $(\mathbf{x}, \mathbf{p})$. Clearly, this collection is a smooth 3-D subset of phase space, which is parameterized by the take-off angles ξ_1, ξ_2 and the flow parameter σ along the bicharacteristics. The tangent vectors in the direction of the ξ_1, ξ_2, and σ-coordinate axes are given by $(\partial\mathbf{x}/\partial\xi_1, \partial\mathbf{p}/\partial\xi_1)$, $(\partial\mathbf{x}/\partial\xi_2, \partial\mathbf{p}/\partial\xi_2)$, and $(\partial\mathbf{x}/\partial\sigma, \partial\mathbf{p}/\partial\sigma)$, respectively. Projecting these vectors to the 3-D physical space, we get $\partial\mathbf{x}/\partial\xi_1$, $\partial\mathbf{x}/\partial\xi_2$, and $\partial\mathbf{x}/\partial\sigma$. The condition $J = 0$ means nothing else than that these vectors are dependent, i.e., that they span a space of dimension lower than three. This implies that the space, spanned by these tangent vectors, has at least one direction which is purely "vertical," i.e., in the $\mathbf{p}$-direction.

As a consequence, the set of bicharacteristics may "turn" in phase space. This situation is illustrated in Figure 7. The solid curve in this figure is a cartoon of the 3-D set of bicharacteristics in phase space. The point $\mathbf{x}_0$ is a caustic point; it is right underneath a point $(\mathbf{x}_0, \mathbf{p}_0)$ where the set of bicharacteristics has a vertical tangent direction. The point $\mathbf{x}'$ exemplifies a point in configuration space where several rays intersect. Notice that at the point of intersection the two rays have different directions given by the slowness vectors $\mathbf{p}(\xi_1^{(1)}, \xi_2^{(1)}, \sigma^{(1)})$ and $\mathbf{p}(\xi_1^{(2)}, \xi_2^{(2)}, \sigma^{(2)})$. Also, at such a point $\mathbf{x}'$ there are two distinct traveltimes $\tilde{\phi}(\xi_1^{(1)}, \xi_2^{(1)}, \sigma^{(1)})$ and $\tilde{\phi}(\xi_1^{(2)}, \xi_2^{(2)}\sigma^{(2)})$ depending on whether the journey from $\mathbf{x}_s$ to $\mathbf{x}'$ is undertaken along the first or the second ray. So once there are caustics, there

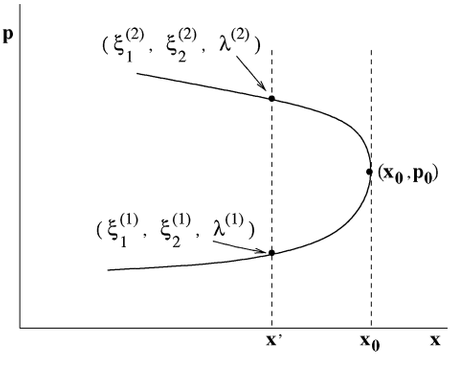

FIG. 7. Turning of the set of bicharacteristics in phase space. At the caustic point $\mathbf{x}_0$, the set of bicharacteristics has a vertical tangent direction.

are several rays in general, all with different slowness vectors $\mathbf{p}^{(i)}$, passing through the same point in physical space. The traveltime function $\tilde{\phi}(\xi_1, \xi_2, \sigma)$ becomes a multivalued function in $\mathbf{x}$-coordinates: $\phi^{(i)}(\mathbf{x}) = \tilde{\phi}(\xi_1^{(i)}, \xi_2^{(i)}, \sigma^{(i)})$. Because of this, and because of the fact that the gradient vectors $\nabla\phi^{(i)}$ jump discontinuously from one branch of the traveltime function to the other, we cannot speak of a classical solution of the eikonal equation anymore. Still, the different branches are important for imaging in complex geologies [see, e.g., ten Kroode et al. (1998) and Operto et al. (2000)].

Figure 8 illustrates the concept of caustics and multivalued traveltime functions in the case of two spatial dimensions. The figure shows a fan of rays originating from a common surface location $(x_s, 0)$. The velocity model is a smoothed version of the well known Marmousi model (Versteeg and Grau, 1991). Also indicated are some wave fronts (i.e. surfaces of constant traveltime) perpendicular to the rays. Clearly, there are regions in the model where several rays pass through the same subsurface location, giving rise to multivalued traveltimes. Also, the wavefronts, which are initially smooth curves, develop singularities in these regions. It can be shown that these singularities, which manifest themselves as the sharp edges of so-called *cusps* are precisely the caustics introduced above.

The solution of the wave equation near caustic points has been carefully analyzed by Hörmander (1971), Duistermaat (1974, 1995) and Maslov and Fedoriuk (1981) from a mathematical point of view, and by Chapman and Drummond (1982) from a more geophysical point of view. It turns out that in a neighborhood of a caustic point one can find a solution of the form

$$G(\mathbf{x}, \mathbf{x}_s, \omega) = \left(\frac{-i\omega}{2\pi}\right)^{3/2} \int d\mathbf{p}\, a(\mathbf{x}, \mathbf{x}_s; \mathbf{p}) e^{i\omega\psi(\mathbf{x}, \mathbf{x}_S; \mathbf{p})}. \tag{86}$$

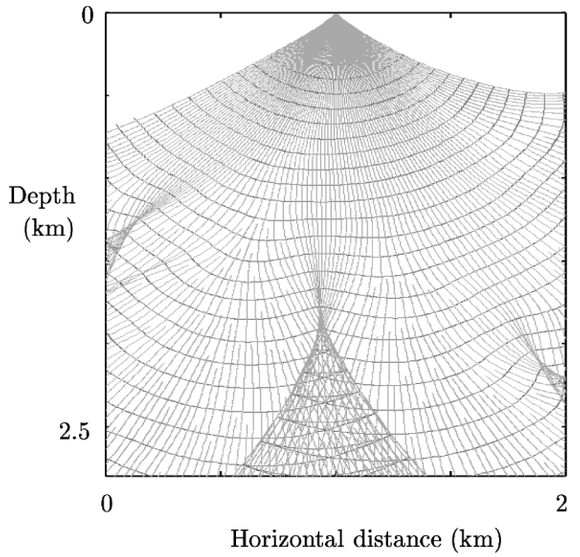

FIG. 8. A fan of rays in two dimensions starting from a surface location and the associated wavefronts. The ray coverage is kept sufficiently high by filling in shadows with new rays (see the section on wavefront construction).

To appreciate the difference with our earlier starting point $G = Ae^{i\omega\phi}$, we try to apply the lemma of stationary phase to the integral in the right-hand side of equation (86). The stationarity conditions are $\nabla_{\mathbf{p}}\psi(\mathbf{x}, \mathbf{x}_s; \mathbf{p}) = 0$, which can be seen as three equations from which we can try to solve for $\mathbf{p}(\mathbf{x}, \mathbf{x}_s)$. If this works, we simply set

$$\phi(\mathbf{x}, \mathbf{x}_s) = \psi(\mathbf{x}, \mathbf{x}_s; \mathbf{p}(\mathbf{x}, \mathbf{x}_s)) \tag{87}$$

and

$$A(\mathbf{x}, \mathbf{x}_s) = a(\mathbf{x}, \mathbf{x}_s; \mathbf{p}(\mathbf{x}, \mathbf{x}_s))/\sqrt{|\det H(\psi)|}, \tag{88}$$

where the *Hessian* of ψ is defined as the matrix of second order derivatives:

$$H(\psi) = \left(\frac{\partial^2\psi}{\partial p_i \partial p_j}\right). \tag{89}$$

Application of the lemma of stationary phase then gives a solution of the form $Ae^{-i\mu\pi/2}e^{i\omega\phi}$, which differs only by a phase factor $e^{-i\mu\pi/2}$ from our earlier starting point (see below for the definition of the number μ). However, according to the implicit function theorem, in order to solve $\mathbf{p}(\mathbf{x}, \mathbf{x}_s)$ from the stationarity conditions, we need to have that $\det H(\psi) \neq 0$. It turns out that this condition is equivalent to the condition $J \neq 0$, which we have found above in our discussion of the method of characteristics for the eikonal equation. In other words, it is not possible to apply the lemma of stationary phase in a caustic point. Fortunately, the integral representation (86) remains valid in a caustic point.

Away from the caustic points, we can solve the stationarity conditions for $\mathbf{p}$ but, as explained above, there will in general be several solutions $\mathbf{p}^{(i)}(\mathbf{x}, \mathbf{x}_s)$, one for each ray from $\mathbf{x}_s$ to $\mathbf{x}$. Hence, we will find a solution of the form

$$G(\mathbf{x}, \mathbf{x}_s, \omega) = \sum_{i=1}^{N} A^{(i)}(\mathbf{x}, \mathbf{x}_s) e^{-i\frac{\pi}{2}\mu^{(i)}} e^{i\omega\phi^{(i)}(\mathbf{x}, \mathbf{x}_S)}, \tag{90}$$

where the integer number

$$\mu^{(i)} = \left[3 - \operatorname{sgn} H\left(\psi\left(\mathbf{x}, \mathbf{x}_s; \mathbf{p}^{(i)}\right)\right)\right]/2 \tag{91}$$

is called the KMAH index. The notation sgn H denotes the signature of the matrix H, i.e., the difference between the number of positive and the number of negative eigenvalues of H. If a ray passes through a caustic point $\mathbf{x}_0$, the determinant of the Hessian goes through zero, which means that one (or two) eigenvalues of $H(\psi)$ change sign. As a consequence, the signature of $H(\psi)$ changes by an even number and the phase in equation (90) changes by an integer multiple of $\pi/2$.

Numerical methods

There are several classes of numerical methods for solving the eikonal and transport equation. We discuss two of them. The first consists of methods which use ray tracing followed by interpolation to a rectangular grid. The second class comprises FD methods.

Numerical ray-trace methods: wavefront construction

In practical applications, one often wants to solve the following problem. Suppose that $\mathbf{x}_s = (x_s, y_s, 0)$ is the location of a seismic source at the surface of the earth, and we want to calculate the traveltime function $\phi(\mathbf{x}, \mathbf{x}_s)$ for all $\mathbf{x}$ on a regular grid. One way of doing this is by shooting a fan of rays starting from the source location $\mathbf{x}_s$, i.e., by solving the ray equations (68) with initial conditions (69) for a range of initial angles $\xi_1^{(k)} = \xi_1^{\min} + (k-1)\Delta\xi_1$, $\xi_2^{(\ell)} = \xi_2^{\min} + (\ell-1)\Delta\xi_2$ (see Figure 8 for a 2-D example).

In fact, it is most convenient to parameterize the ray equations by time t instead of the flow parameter σ. Since $d\phi/d\sigma = \mathbf{p}^2 = 1/c^2$, the reparameterized equations become

$$\frac{d\mathbf{x}}{dt} = c^2\mathbf{p}, \qquad \frac{d\mathbf{p}}{dt} = -c^{-1}\nabla c, \qquad \frac{d\phi}{dt} = 1. \tag{92}$$

The equations are usually solved numerically by a Runge-Kutta method. The result is a family of points $\mathbf{x}_{k\ell m} = \mathbf{x}(\xi_1^{(k)}), \mathbf{x}(\xi_2^{(\ell)}), m\Delta t$. For fixed indices k and ℓ, these points are on an individual ray characterized by the initial angles $\xi_1^{(k)}, \xi_2^{(\ell)}$. For fixed index m, they form a discretization of a wavefront at time $t = m\Delta t$.

The half space $z > 0$ is then divided into prisms with vertices $\mathbf{x}_{k,\ell,m}$, $\mathbf{x}_{k+1,\ell,m}$, $\mathbf{x}_{k,\ell+1,m}$, $\mathbf{x}_{k,\ell,m+1}$, $\mathbf{x}_{k+1,\ell,m+1}$, and $\mathbf{x}_{k,\ell+1,m+1}$. If a point $\mathbf{x}$ is inside such a prism, one interpolates the traveltime in $\mathbf{x}$ trilinearly from the known values at the vertices. This concept of shooting a fan of rays and then interpolating in prisms is widely applied in practice. Obviously, the interpolation tends to become somewhat inaccurate if two neighboring rays, which are initially close to each other, start to diverge strongly. This is partly a natural process as time increases (consider, e.g., the constant velocity case where rays are radii from a sphere centered at the source location); partly it may also be caused by strong variations in the velocity. For example, high-velocity regions tend to act as diverging lenses for a fan of rays. In order to get accurate traveltimes for such situations, Vinje et al. (1993) introduced the concept of wavefront construction. The essence of this method is that, whenever the three points $\mathbf{x}_{k,\ell,m}$, $\mathbf{x}_{k+1,\ell,m}$, and $\mathbf{x}_{k,\ell+1,m}$ are too far apart, a new ray is started on the wavefront $t = m\Delta t$ starting from a location between these three points. In this way, one will get an even distribution of the subsurface with rays. This method has been used in the computation of the result shown in Figure 8.

Notice that this method is quite capable of calculating multivalued traveltime functions, because a given point $\mathbf{x}$ can be in several prisms. Each of those yields an interpolated traveltime at $\mathbf{x}$.

Obviously, one need not restrict the interpolation to traveltimes. All other quantities computed during the ray tracing are known at the vertices $\mathbf{x}_{k\ell m}$ and can be interpolated in the same way. In particular, one can calculate the amplitudes $A(\mathbf{x}, \mathbf{x}_s)$ of the Green's function on a regular grid. Just as the traveltime, the amplitude function will be multivalued at a point $\mathbf{x}$, if $\mathbf{x}$ lies in several prisms. In this way we can calculate, for example, the asymptotic Green's function given in equation (90) associated with the fan of rays in Figure 8 at the bottom of the model ($z = 2900$ m). Obviously, the amplitudes blow up in the neighborhood of caustics, where one should use the representation (86). Taking this for granted, and convolving with a 50-Hz Gabor wavelet, one obtains the result plotted in Figure 9. Notice that most of the energy is in the later arrivals.

FD methods

Instead of using a ray-tracing method, one can also solve the eikonal and the transport equations directly by using FD methods. The methods we describe here are the essentially non-oscillatory (ENO) upwind FD methods. These methods were introduced by Osher and Sethian (1988) for a general class of first-order partial differential equations. Further work on the eikonal equation was done by Vidale (1988, 1990), Van Trier and Symes (1991), El-Majeed et al. (1997), Kim and Cook (1999), and Qian and Symes (1999).

The advantage of FD methods (as opposed to ray-tracing methods) is that they calculate the traveltime field $\phi(\mathbf{x})$ directly on a grid, so there is no need for interpolation. Also, no special precautions have to be taken in shadow zones, unlike the wavefront construction method described above, which shoots additional rays in these regions in order to keep an even ray coverage. Therefore, FD eikonal solvers are computationally very efficient.

Multivaluedness is, however, not so easily incorporated into an FD eikonal solver. In fact, most FD eikonal solvers calculate the so-called viscosity solution, introduced in the mathematical literature by Crandall and Lions (1983). The idea is roughly as follows. If one adds a viscosity term $-\epsilon\Delta\phi$ to the eikonal equation (56), there is a unique smooth (and, in particular, single-valued) solution ϕ_ϵ. The viscosity solution is then the limit, in a weak sense, $\lim_{\epsilon\downarrow 0}\phi_\epsilon$. It turns out that the viscosity solution coincides with the first arrival from the source to the location $\mathbf{x}$.

The nature of this first-arrival or viscosity solution is illustrated in Figure 10, which shows the propagation of first-arrival wavefronts for the same model and shot as used for the calculation of rays and wavefronts in Figure 8. Comparing Figures 8 and 10, one sees that the cusps (corresponding to the later arrivals) are missing from the wavefronts. Notice that the first-arrival wavefronts in Figure 10 have points where their

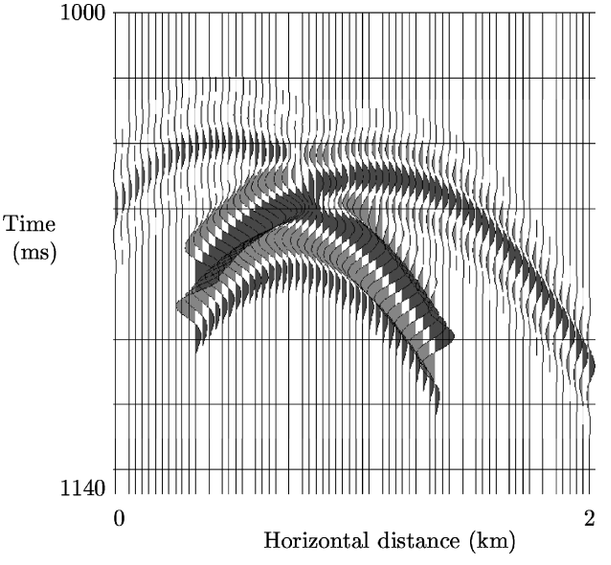

FIG. 9. Green's function (convolved with a 50-Hz Gabor wavelet) for the fan of rays from Figure 8 evaluated at $z = 2900$ m and at 25-m x intervals.

gradient vector is discontinuous; these correspond to the self-intersections of the true wavefronts (Figure 8) and are called shocks.

Let us briefly discuss the general structure of an upwind FD method for the eikonal equation. First, one solves the z-component of the traveltime gradient from the eikonal equation by choosing

$$\frac{\partial \phi}{\partial z} = \sqrt{\frac{1}{c^2} - \left(\frac{\partial \phi}{\partial x}\right)^2 - \left(\frac{\partial \phi}{\partial y}\right)^2}. \tag{93}$$

Obviously, the choice of the positive root means that we are restricting ourselves to rays propagating downwards, which is not a serious limitation for many applications. Another consequence is that we have to take precautions in order to guarantee that the argument of the square root remains positive. The argument can become negative if the angle θ that a ray makes with the positive z-axis becomes too large. The remedy is to replace the argument by $\cos^2(\theta_{\max})/c^2$ if $c^{-1}(\phi_x^2 + \phi_y^2) > \sin^2(\theta_{\max})$. Effectively, this amounts to accurate traveltime calculation inside a cone $|\theta| < \theta_{\max}$.

If we denote the right-hand side of equation (93) by $F(c, \partial_x\phi, \partial_y\phi)$ and write ϕ_{ij}^k for the value of the traveltime on the grid point $(i\Delta x,\ j\Delta y, k\Delta z)$, we can write

$$\phi_{ij}^{k+1} \cong \phi_{ij}^k + \Delta z F\left(c_{ij}^k, (\partial_x\phi)_{ij}^k, (\partial_y\phi)_{ij}^k\right) \tag{94}$$

and solve for ϕ_{ij}^{k+1} recursively. If one wants higher order accuracy, one should, of course, use a higher order scheme for the z-integration.

The essence of the method is the specification of how to calculate the derivatives $\partial_x\phi$ and $\partial_y\phi$ in the right-hand side of equation (94) by finite differences. This is done by choosing an ingeneous combination of the standard first order FD operators:

$$\begin{aligned} D_x^{\pm}\phi(x,y,z) &= \pm\frac{\phi(x \pm \Delta x, y, z) - \phi(x,y,z)}{\Delta x}, \\ D_y^{\pm}\phi(x,y,z) &= \pm\frac{\phi(x, y \pm \Delta y, z) - \phi(x,y,z)}{\Delta y}. \end{aligned} \tag{95}$$

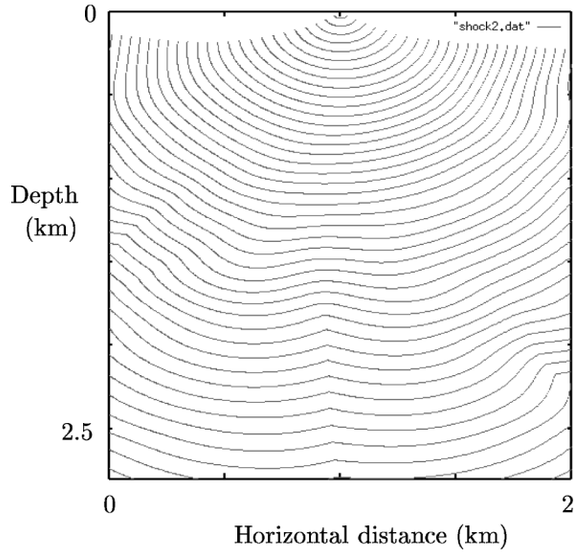

FIG. 10. Propagation of first-arrival wavefronts for the same shot and model as used in Figure 8.

For a first-order scheme, for example, one takes

$$\partial_x\phi \cong \max|\max(D_x^-\phi, 0), \min(D_x^+\phi, 0)|, \tag{96}$$

and similarly for the y-derivative. These FD operators are such that only upwind (i.e., in the direction from which the rays are coming) information is used to approximate the derivative. To see this, we discern the four cases: (1) $D_x^-\phi > 0$, $D_x^+\phi > 0$, (2) $D_x^-\phi < 0$, $D_x^+\phi < 0$, (3) $D_x^-\phi < 0$, $D_x^+\phi > 0$, and (4) $D_x^-\phi > 0$, $D_x^+\phi < 0$.

Case 1 corresponds to the situation where all rays intersecting a certain depth level z in an x-interval $[x - \Delta x, x + \Delta x]$ travel from left to right. The right-hand side of equation (96) is then equal to $D_x^-\phi$, which is indeed an upwind finite difference. The second case corresponds to the situation where all rays in the interval $[x - \Delta x, x + \Delta x]$ travel from right to left, and again the difference operator (96) picks the upwind difference. In case 3, the right-hand side of equation (96) vanishes. This case corresponds to the situation where the rays passing through the interval $[x - \Delta x, x + \Delta x]$ at depth z change direction: first they all move from left to right, then they move from right to left. Presumably, $\mathbf{x}$ is then close to a point of rarefaction, and the derivative $\partial_x\phi$ is indeed zero up to first order. Finally, case 4 corresponds to the situation where there is a shock on the interval $[x - \Delta x, x + \Delta x]$ (see Figure 10 for an illustration). In principle there are now two rays arriving in the point $(x, y, z + \Delta z)$, so we could choose two different traveltimes. The choice maxmod $(D_x^-\phi, D_x^+\phi, 0)$ to approximate the derivative $\partial_x\phi$ turns out to select the shortest traveltime (see Qian and Symes, 1999).

For practical purposes, first-order schemes are very inefficient. Moreover, if one also wants to solve the transport equation by finite differences, one needs to have higher order accuracy for the traveltimes. For this purpose, one can use the ENO methods mentioned before. They differ from the first-order method described above by a more complicated prescription of the difference operators than the one given in equation (96), which is accurate up to higher order [see Osher and Sethian (1988) and Kim and Cook (1999)].

The fact that no later arrivals are calculated is a disadvantage for some applications, such as multivalued imaging. Symes (1996) and Benamou (1999) adapted the standard FD methods in such a way that they calculate multivalued arrival times when these occur.

Interfaces

Until now, we have implicitly assumed that our velocity model $c(\mathbf{x})$ is smooth (i.e., that it does not contain jump discontinuities). The theory of asymptotics is most easily explained in such a medium. The asymptotic solutions in smooth media, and in particular the traveltime and amplitude functions $\phi(\mathbf{x}, \mathbf{x}_s)$ and $A(\mathbf{x}, \mathbf{x}_s)$, can be used in transmission tomography and migration using a smooth background model (see, e.g., Cohen et al, 1986).

Most geological subsurface models, however, contain discontinuities. After all, this is the reason that we can probe the subsurface by surface seismic techniques in the first place. Asymptotic techniques are easily extended to models with interfaces of discontinuities. Assuming that the interface divides the subsurface into two regions, each with its own smooth

velocity function, say $c_1(\mathbf{x})$ and $c_2(\mathbf{x})$, we write

$$G(\mathbf{x}, \mathbf{x}_s, \omega) = A_{in}(\mathbf{x}, \mathbf{x}_s)e^{i\omega\phi_{in}(\mathbf{x},\mathbf{x}_S)} + A_{refl}(\mathbf{x}, \mathbf{x}_s)e^{i\omega\phi_{refl}(\mathbf{x},\mathbf{x}_S)} \quad (97)$$

on one side of the interface and

$$G(\mathbf{x}, \mathbf{x}_s, \omega) = A_{refr}(\mathbf{x}, \mathbf{x}_s)e^{i\omega\phi_{refr}(\mathbf{x},\mathbf{x}_S)} \quad (98)$$

on the other side. Here, ϕ_{in} and ϕ_{refl} satisfy the eikonal equation for the velocity function $c_1(\mathbf{x})$, while ϕ_{refr} is a solution of the eikonal equation for the velocity function $c_2(\mathbf{x})$. The physical interpretation of the above is that one has an incoming and a reflected wave on one side of the interface and a refracted wave on the other side.

To proceed, one requires continuity of the solution G and its normal derivative $\mathbf{n}\cdot\nabla G$ at the interface of discontinuity. These two conditions lead to Snell's reflection/refraction laws for the rays. Integrating along reflected/refracted rays will provide us with reflected/refracted traveltimes ϕ_{refl} and ϕ_{refr}. Moreover, they enable us to express the amplitudes $A_{refl}(\mathbf{x}, \mathbf{x}_s)$ and $A_{refr}(\mathbf{x}, \mathbf{x}_s)$ at the interface in terms of the amplitude $A_{in}(\mathbf{x}, \mathbf{x}_s)$. Integrating the transport equation along reflected/refracted rays will provide us with the amplitudes $A_{refl}(\mathbf{x}, \mathbf{x}_s)$ and $A_{refr}(\mathbf{x}, \mathbf{x}_s)$ away from the interface.The details of the calculation can be found e.g in Červený et al. (1977) and Červený (1985, 1987), or Bleistein (1984).

CONCLUSIONS

The direct methods discussed in this review (finite differences, pseudospectral methods, and finite-element methods) do not have restrictions on the type of constitutive equation, boundary conditions, and source-type, and allow general material variability. For instance, the numerical solution of wave propagation in an anisotropic poro-viscoelastic medium (appropriate for reservoir environments) is not particularly difficult in comparison with simple cases, such as the acoustic wave equation describing the propagation of dilatational waves. Many of the complex constitutive equations handled by direct methods cannot be solved by integral-equation or asymptotic methods without simplifying assumptions. However, direct methods for solving these equations are certainly more expensive in terms of computer time and storage requirements.

Finite differences are simple to program and are efficient when compared to alternative methods in cases where the accuracy requirements are fairly mild. In this sense, a good choice can be an FD algorithm which is second order in time and fourth order in space. Pseudospectral methods can be more expensive in some cases, but guarantee high accuracy and relatively lower background noise when staggered differential operators are used. These operators are also suitable when large variations of Poisson's ratio are present in the model (e.g., a fluid-solid interface). In three dimensions, pseudospectral methods require a minimum of grid points and can be the best choice when limited computer storage is available. However, if a dense grid is required for physical reasons (e.g., fine layering, scattering inhomogeneities, etc.) the FD algorithm can be more convenient.

Without doubt, the best algorithm to model surface topography and curved interfaces is the FE method. With the use of spectral interpolators, this algorithm can compete with the previous techniques as regards accuracy and stability. However, FE methods may prove to be unstable for large variations of the Poisson's ratio. FE methods are best suited for engineering problems, where interfaces are well defined (in contrast with geological interfaces). Accurate modeling of topography or interfaces often requires the use of nonstructured grids. Especially in three dimensions, this is one of the main disadvantages of FE methods because of the geometrical problems to be solved when constructing the model. FE methods, however, are to be preferred for seismic problems involving the propagation of surface waves in situations of complex topography.

Integral-equation methods are based on integral representations of the wavefield. These representations contain a Green's function that accounts for wave propagation in the embedding medium. For specific geometries (such as boreholes or other boundaries, media containing cracks, and inclusions of bounded extent), these methods can be relatively efficient as compared to direct methods. The reason for this efficiency is that the number of unknown functions to be determined is confined to a bounded region. The price to pay for this reduction in unknowns is the fact that the system matrix is full, whereas direct methods usually have sparse system matrices that can be solved in an efficient way. Since integral-equation methods can explicitly account for the boundary conditions at crack boundaries or borehole walls, these methods can provide accurate results for those specific geometries including irregular boreholes or boundaries, media containing cracks, and inclusions of bounded extent. Also, for deriving analytical imaging methods, integral-equation techniques are very well suited, and are often used together with asymptotic methods.

Asymptotic methods aim at the calculation of approximate solutions for the wave equation that are valid for high frequencies. Asymptotic methods calculate the solution up to a smooth error. In fact, they calculate only the most singular part of the solution, which is characterized by a traveltime function and an amplitude function. The traveltime function is a solution of the eikonal equation; the amplitude function is a solution of the transport equation. These equations can be solved in several ways. Wavefront construction and ENO upwind FD schemes are two of the most important ones. Both methods are very efficient in terms of CPU usage.

Due to their computational efficiency, asymptotic methods are widely applied in the generation of synthetic seismograms and the solution of inverse problems such as traveltime tomography and migration.

ACKNOWLEDGMENTS

First of all, the authors acknowledge the support and comments from Sven Treitel and the critical but very important reviews of Norm Bleistein and Johann Robertsson. Figures 1 and 4 were taken from Huygens' famous *Traité de la lumière*, which was reprinted in 1990 (together with the original French version). We gratefully acknowledge Epsilon, Utrecht, for giving us permission to use these illustrations.

REFERENCES

Aki, K., and Richards, P. G., 1980, Quantitative seismology: W. H. Freeman and Co.

Alterman, Z., and Karal, Jr., F. C., 1968, Propagation of elastic waves in layered media by finite-difference methods: Bull. Seism. Soc. Am., **58**, 367–398.

Bayliss, A., Jordan, K. E., LeMesurier, B. J., and Turkel, E., 1986, A fourth-order accurate finite-difference scheme for the computation of elastic waves: Bull. Seism. Soc. Am., **76**, 1115–1132.
Baysal, E., Kosloff, D. D., and Sherwood, J. W. C., 1984, A two-way nonreflecting wave equation: Geophysics, **49**, 132–141.
Benamou, J.-D., 1999, Direct solution of multi valued phase space solutions for Hamilton-Jacobi equations: Comm. Pure and Appl. Math., **52**, 1443–1475.
Bennett, C. L., and Mieras, H., 1981, Time domain integral equation solution for acoustic scattering from fluid targets: J. Acoust. Soc. Am., **69**, 1261–1265.
Berenger, J. P., 1994, A perfectly matched layer for the absorption of electromagnetic waves: J. Comput. Phys., **114**, 185–200.
Blanch, J. O., and Robertsson, J. O. A., 1997, A modified Lax-Wendroff correction for wave propagation in media described by Zener elements: Geophys. J. Internat., **111**, 381–386.
Bleistein, N., 1984, Mathematical methods for wave phenomena: Academic Press.
Bleistein, N., Cohen, J. K., and Stockwell, Jr., J. W., 2001, Mathematics of multidimensional seismic imaging, migration and inversion: Springer.
Bouchon, M., 1987, Diffraction of elastic waves by cracks or cavities using the discrete wavenumber method: J. Acoust. Soc. Am., **81**, 1671–1676.
Bouchon, M., and Schmidt, D. P., 1989, Full-wave acoustic logging in an irregular borehole: Geophysics, **54**, 758–765.
Carcione, J. M., 1991, Domain decomposition for wave propagation problems: J. Sci. Comput., **6**, 453–472.
——— 1992, Modeling anelastic singular surface waves in the earth: Geophysics, **57**, 781–792.
——— 1994a, The wave equation in generalized coordinates: Geophysics, **59**, 1911–1919.
——— 1994b, Time-dependent boundary conditions for the 2-D linear anisotropic-viscoelastic wave equation: Numer. Meth. Part. Diff. Equations, **10**, 771–791.
Carcione, J. M., and Helle, H. B., 1999, Numerical solution of the poroviscoelastic wave equation on a staggered mesh: J. Comput. Phys., **154**, 520–527.
Carcione, J. M., Kosloff, D., and Kosloff, R., 1988, Viscoacoustic wave propagation simulation in the earth: Geophysics, **53**, 769–777.
Carcione, J. M., and Quiroga-Goode, G., 1996, Some aspects of the physics and numerical modeling of Biot compressional waves: J. Comput. Acous., **3**, 261–280.
Celia, M. A., and Gray, W. G., 1992, Numerical methods for differential equations: Fundamental concepts for scientific and engineering applications: Prentice-Hall.
Cerjan, C., Kosloff, D., Kosloff, R., and Reshef, M., 1985, A nonreflectng boundary condition for discrete acoustic and elastic wave equations: Geophysics, **50**, 705–708.
Červený, V., 1985, The application of raytracing to the propagation of shear waves in complex media: Geophysical Press.
——— 1987, Ray methods for three dimensional seismic modelling: Lecture notes for the petroleum industry course at the Norwegian Institute of Technology.
Červený, V., Molotkov, I., and Pšenčik, I., 1977, Ray method in seismology: Univ. Karlova.
Chapman, C. H., and Drummond, R., 1982, Body-wave seismograms in inhomogeneous media using Maslov asymptotic theory: Bull. Seism. Soc. Am., **72**, S277–S317.
Chew, W. C., and Liu, Q. H., 1996, Perfectly matched layers for elastodynamics: A new absorbing boundary condition: J. Comput. Acous., **4**, 341–359.
Clayton, R., and Engquist, B., 1977, Absorbing boundary conditions for acoustic and elastic wave equations: Bull. Seism. Soc. Am., **67**, 1529–1540.
Cohen, J. K., Hagin, F. G., and Bleistein, N., 1986, Three-dimensional Born inversion with an arbitrary reference: Geophysics, **51**, 1552–1558.
Courant, R., and Hilbert, D., 1937, Methoden der Mathematischen Physik II: Julius Springer.
——— 1966, Methods of mathematical physics, vol. II, Interscience [English translation of Courant and Hilbert (1937)].
Crandall, M., and Lions, P., 1983, Viscosity solutions of Hamilton-Jacobi equations: Trans. Am. Math. Soc., **277**, 1–42.
Dablain, M. A., 1986, The application of high-order differencing to the scalar wave equation: Geophysics, **51**, 54–66.
Dai, N., Vafidis, A., and Kanasewich, E. R., 1995, Wave propagation in heterogeneous, porous media: A velocity-stress, finite-difference method: Geophysics, **60**, 327–340.
De Hoop, A. T., 1995, Handbook of radiation and scattering of waves: Academic Press.
Dong, W., Bouchon, M., and Toksoz, M. N., 1995, Borehole seismic-source radiation in layered isotropic and anisotropic media: Boundary element modeling: Geophysics, **60**, 735–747.
Duistermaat, J. J., 1974, Oscillatory integrals, Lagrange immersions and unfolding of singularities: Comm. Pure and Appl. Math., **27**, 207–281.
Duistermaat, J. J., 1995, Fourier integral operators: Birkhäuser.
El-Mageed, M. A., Kim, S., and Symes, W. W., 1997, 3-D Kirchhoff migration using finite difference traveltimes and amplitudes: The Rice Inversion Project, Annual Report, paper no. 5.
Emmerich, H., 1989, 2-D wave propagation by a hybrid method, Geophys. J. Internat., **99**, 307–319.
Emmerich, H., and Korn, M., 1987, Incorporation of attenuation into time-domain computations of seismic wave fields: Geophysics, **52**, 1252–1264.
Emerman, S. H., Schmidt, W., Stephen, R. A., 1982, An implicit finite-difference formulation of the elastic wave equation: Geophysics, **47**, 1521–1526.
Fagin, S. W., 1992, Seismic modeling of geological structures: Applications to exploration problems: Soc. Expl. Geophys.
Fokkema, J. T., 1980, Reflection and transmission of elastic waves by the spatially periodic interface between two solids (theory of the integral-equation method): Wave Motion **2**, 375–393.
Fornberg, B., 1988, The pseudospectral method: accurate representation of interfaces in elastic wave calculations: Geophysics, **53**, 625–637.
Fornberg, B., 1996, A practical guide to pseudospectral methods: Cambridge Univ. Press.
Gazdag, J., 1981, Modeling the acoustic wave equation with transforms methods: Geophysics, **54**, 195–206.
Gottlieb, D., and Orszag, S. A., 1977, Numerical analysis of spectral methods: Soc. Ind. Appl. Math.
Harrington, R. F., 1968, Field computation by moment methods: Macmillan Co.
Higdon, R. L., 1991, Absorbing boundary conditions for elastic waves: Geophysics, **56**, 231–241.
Holberg, O., 1987, Computational aspects of the choice of operator and sampling interval for numerical differentiation in large-scale simulation of wave phenomena: Geophys. Prosp., **35**, 629–655.
Hörmander, L., 1971, Fourier integral operators I: Acta Mathematica, **127**, 79–183.
Hughes, T. J. R., 1987, The finite element method: Prentice-Hall International, Inc.
Huygens, C., 1990, Verhandeling over het licht (Dutch translation by D. Eringa of Traité de la lumière, together with the original 1690 French version): Epsilon.
Igel, H., 1999, Wave propagation in three-dimensional spherical sections by the Chebyshev spectral method: Geophys. J. Internat., **139**, 559–566.
Igel, H., Mora, P., and Riollet, B., 1995, Anisotropic wave propagation through finite-difference grids: Geophysics, **60**, 1203–1216.
Jain, M. K., 1984, Numerical solutions of differential equations: Wiley Eastern Ltd.
Jo, C.-H., Shin, C., and Suh, J. H., 1996, An optimal 9-point finite-difference, frequency-space, 2-D scalar wave extrapolator: Geophysics, **61**, 529–537.
Karrenbach, M., 1998, Full wave form modelling in complex media: 68th Ann. Internat. Mtg., Soc. Expl. Geophys., Expanded Abstracts, 1444–1447.
Kelly, K. R., and Marfurt, K. J., Eds., 1990, Numerical modeling of seismic wave propagation: Soc. Expl. Geophys.
Kelly, K. R., Ward, R. W., Treitel, S., and Alford, R. M., 1976, Synthetic seismograms: A finite-difference approach: Geophysics, **41**, 2–27.
Kessler, D., and Kosloff, D., 1991, Elastic wave propagation using cylindrical coordinates: Geophysics, **56**, 2080–2089.
Keys, R. G., 1985, Absorbing boundary conditions for acoustic media: Geophysics, **50**, 892–902.
Kim, S., and Cook, R., 1999, 3-D traveltime computation using second order ENO scheme: Geophysics, **64**, 1867–1876.
Kneib, G., and Kerner, C., 1993, Accurate and efficient seismic modeling in random media: Geophysics, **58**, 576–588.
Komatitsch, D., and Vilotte, J. P., 1998, The spectral element method: An efficient tool to simulate the seismic response of 2D and 3D geological structures: Bull. Seis. Soc. Am., **88**, 368–392.
Kosloff, D., and Baysal, E., 1982, Forward modeling by the Fourier method: Geophysics, **47**, 1402–1412.
Kosloff, D., and Kessler, D., 1989, Seismic numerical modeling, *in* Desaubies, Y., Tarantola, A., and Zinn-Justin, J., Eds., Oceanographic and geophysical tomography: North-Holland, 249–312.
Kosloff, D., Kessler, D., Queiroz Filho, A., Tessmer, E., Behle, A., and Strahilevitz, R., 1990, Solution of the equation of dynamic elasticity by a Chebychev spectral method: Geophysics, **55**, 734–748.
Kosloff, D., and Kosloff, R., 1986, Absorbing boundaries for wave propagation problems: J. Comput. Phys., **63**, 363–376.

Kosloff, D., Queiroz Filho, A., Tessmer, E., and Behle, A., 1989, Numerical solution of the acoustic and elastic wave equations by a new rapid expansion method: Geophys. Prosp., **37**, 383–394.
Kosloff, D., Reshef, M., and Loewenthal, D., 1984, Elastic wave calculations by the Fourier method: Bull. Seism. Soc. Am., **74**, 875–891.
Levander, A. R., 1988, Fourth-order finite-difference *P–SV* seismograms: Geophysics, **53**, 1425–1436.
——— 1989, Finite-difference forward modeling in seismology, *in* James, D. E., Ed., The encyclopedia of solid earth geophysics: Van Nostrand Reinhold, 410–431.
Liu, E., Crampin, S., and Hudson, J. A., 1997, Diffraction of seismic waves by cracks with application to hydraulic fracturing: Geophysics, **62**, 253–265.
Loewenthal, D., Lu, L., Roberson, R., and Sherwood, J. W. C., 1976, The wave equation applied to migration: Geophys. Prosp., **24**, 380–399.
Lysmer, J., and Drake, L. A., 1972, A finite element method for seismology, *in* Alder, B., Fernbach, S., and Bolt, B. A., Eds., Methods in computational physics II, Seismolgy: Academic Press, 181–216.
Marfurt, K. J., 1984, Accuracy of finite-difference and finite-element modeling of the scalar and elastic wave equations: Geophysics, **49**, 533–549.
Maslov, V. P., and Fedoriuk, M. V., 1981, Semi-classical approximation in quantum mechanics: Reidel.
Mikhailenko, B. G., 1985, Numerical experiment in seismic investigation: J. Geophys., **58**, 101–124.
Moczo, P., 1989, Finite-difference techniques for *SH*-waves in 2-D media using irregular grids—Application to the seismic response problem: Geophys. J. Internat., **99**, 321–329.
Moczo, P., Bystrický, E., Kristek, J., Carcione, J. M., and Bouchon, M., 1997, Hybrid modelling of *P–SV* seismic motion at inhomogeneous viscoelastic topographic viscoelastic structures: Bull. Seism. Soc. Am., **87**, 1305–1323.
Mora, P., 1989, Modeling anisotropic seismic waves in 3-D: 59th Ann. Internat. Mtg., Soc. Expl. Geophys., Expanded Abstracts, **2**, 1039–1043.
Mufti, I. R., 1985, Seismic modeling in the implicit mode: Geophys. Prosp., **33**, 619–656.
Muijres, A. J. H., Herman, G. C., and Bussink, P. G. J., 1998, Acoustic wave propagation in two-dimensional media containing small-scale heterogeneities: Wave Motion, **27**, 137–154.
Muir, F., Dellinger, J., Etgen, J., and Nichols, D., 1992, Modeling elastic wavefields across irregular boundaries: Geophysics, **57**, 1189–1193.
Operto, S., Xu, S., and Lambare, G., 2000, Can we quantitively image complex models with rays?: Geophysics, **65**, 1223–1238.
Opršal, I., and Zahradnik, J., 1999, Elastic finite-difference method for irregular grids: Geophysics, **64**, 240–250.
Osher, S., and Sethian, J. A., 1988, Fronts propagating with curvature dependent speed: Algorithms based on Hamilton-Jacobi formulations: J. Comp. Physics, **79**, 12–49.
Özdenvar, T., and McMechan, G., 1997, Algorithms for staggered-grid computations for poroelastic, elastic, acoustic, and scalar wave equations: Geophys. Prosp., **45**, 403–420.
Özdenvar, T., McMechan, G., and Chaney, P., 1996, Simulation of complete seismic surveys for evaluation of experiment design and processing: Geophysics, **61**, 496–508.
Padovani, E., Priolo, E., and Seriani, G., 1994, Low- and high-order finite element method: experience in seismic modeling: J. Comp. Acoust., **2**, 371–422.
Pao, Y. H., and Varatharajulu, V., 1976, Huygens' principle, radiation conditions, and integral formulas for the scattering of elastic waves: J. Acoust. Soc. Am., **59**, 1361–1371.
Pointer, T., Liu, E., and Hudson, J. A., 1998, Numerical modelling of seismic waves scattered by hydrofractures: Application of the indirect boundary element method: Geophys. J. Internat., **135**, 289–303.
Priolo, E., Carcione, J. M., and Seriani, G., 1994, Numerical simulation of interface waves by high-order spectral modeling techniques: J. Acoust. Soc. Am., **95**, 681–693.
Qian, J., and Symes, W. W., 1999, Upwind finite difference traveltime for anisotropic media: The Rice Inversion Project, Annual Report, paper no. 2.
Randall, C. J., 1988, Absorbing boundary condition for the elastic wave equation: Geophysics, **53**, 611–624.
Reshef, M., Kosloff, D., Edwards, M., and Hsiung, C., 1988, Three-dimensional elastic modeling by the Fourier method: Geophysics, **53**, 1184–1193.
Robertsson, J. O. A., 1996, A numerical free-surface condition for elastic/viscoelastic finite-difference modeling in the presence of topography: Geophysics, **61**, 1921–1934.
Robertsson, J. O. A., Blanch, J. O., and Symes, W. W., 1994, Viscoelastic finite-difference modeling: Geophysics, **59**, 1444–1456.
Robertsson, J. O. A., and Chapman, C. H., 2000, An efficient method for calculating finite-difference seismograms after model alterations: Geophysics, **65**, 907–918.
Robertsson, J. O. A., Levander, A., and Holliger, K., 1996, A hybrid wave propagation simulation technique for ocean acoustic problems: J. Geophys. Res., **101**, 11225–11241.
Santos, J. E., Douglas, Jr., J., Morley, M. E., and Lovera, O. M., 1988, Finite element methods for a model for full waveform acoustic logging: J. Numerical Analysis, **8**, 415–433.
Sarma, G. S., Mallick, K., and Gadhinglajkar, V. R., 1998, Nonreflecting boundary condition in finite-element formulation for an elastic wave equation: Geophysics, **63**, 1006–1016.
Schlue, J. W., 1979, Finite element matrices for seismic surface waves in three-dimensional sructures: Bull. Seism. Soc. Am., **69**, 1425–1438.
Seriani, G., Priolo, E., Carcione, J. M., and Padovani, E., 1992, High-order spectral element method for elastic wave modeling: 62nd Ann. Internat. Mtg., Soc. Expl. Geophys., Expanded Abstracts, 1285–1288.
Serón, F. J., Badal, J., and Sabadell, F. J., 1996, A numerical laboratory for simulation and visualization of seismic wavefields: Geophys. Prospect., **44**, 603–642.
Serón, F. J., Sanz, F. J., Kindelan, M., and Badal, J. I., 1990, Finite-element method for elastic wave propagation: Comm. Appl. Numerical Methods, **6**, 359–368.
Smith, G. D., 1985, Numerical solution of partial differential equations: Finite difference methods, Clarendon Press.
Stead, R. J., and Helmberger, D. V., 1988, Numerical-analytical interfacing in two dimensions with applications to modeling NTS seismograms: Pageoph, **128**, 157–193.
Symes, W. W., 1996, A slowness matching finite difference method for traveltimes beyond caustics: The Rice Inversion Project, Annual Report, paper no. 8.
Tal-Ezer, H., Carcione, J. M., and Kosloff, D., 1990, An accurate and efficient scheme for wave propagation in linear viscoelastic media: Geophysics, **55**, 1366–1379.
Tal-Ezer, H., Kosloff, D., and Koren, Z., 1987, An accurate scheme for seismic forward modeling: Geophys. Prosp., **35**, 479–490.
Tan, T. H., 1976, Diffraction of time-harmonic elastic waves by a cylindrical obstacle: Appl. Sci. Res., **32**, 97–144.
ten Kroode, A. P. E., Smit, D.-J., and Verdel, A. R., 1998, A microlocal analysis of migration: Wave Motion, **28**, 149–172.
Tessmer, E., Kessler, D., Kosloff, D., and Behle, A., 1992, Multi-domain Chebyshev-Fourier method for the solution of the equations of motion of dynamic elasticity: J. Comput. Phys., **100**, 355–363.
Tessmer, E., and Kosloff, D., 1994, 3-D elastic modeling with surface topography by a Chebychev spectral method: Geophysics, **59**, 464–473.
Ursin, B., 1983, Review of elastic and electromagnetic wave propagation in horizontally layered media: Geophysics, **48**, 1063–1081.
Vafidis, A., Abramovici, F., and Kanasewich, E. R., 1992, Elastic wave propagation using fully vectorized high order finite-difference algorithms: Geophysics, **57**, 218–232.
Van Trier, J., and Symes, W. W., 1991, Upwind finite difference calculations of traveltimes: Geophysics, **56**, 812–821.
Versteeg, R. J., and Grau, G., Eds., 1991, The Marmousi experience: Proc. 1990 EAGE workshop on practical aspects of seismic data inversion: Eur. Assn. Geosci. Eng.
Vidale, J. E., 1988, Finite difference calculation of traveltimes: Bull. Seism. Soc. Am., **78**, 2062–2076.
——— 1990, Finite difference calculation of traveltimes in three dimensions: Geophysics, **55**, 521–526.
Vinje, V., Iversen, E., and Gjøstal, H., 1993, Traveltime and amplitude estimation using wavefront construction: Geophysics, **58**, 1157–1166.
Virieux, J., 1986, *P–SV* wave propagation in heterogeneous media: Velocity-stress finite-difference method: Geophysics, **51**, 888–901.
Zeng, X., and West, G. F., 1996, Reducing spurious diffractions in elastic wavefield calculations: Geophysics, **61**, 1436–1439.
Zhang, C., and LeVeque, R. J., 1997, The immersed interface method for acoustic wave equations with discontinuous coefficients: Wave Motion, **25**, 237–263.
Zienkiewicz, O. C., 1977, The finite element method, 3rd ed.: McGraw-Hill Book Co.